cmgh
CELLULAR AND MOLECULAR GASTROENTEROLOGY AND HEPATOLOGY

ORIGINAL RESEARCH

Aryl Hydrocarbon Receptor Deficiency in Intestinal Epithelial Cells Aggravates Alcohol-Related Liver Disease

Minyi Qian,[1,2,3,*] Jun Liu,[1,2,*] Danyang Zhao,[1,2,*] Pengpeng Cai,[4,*] Chuyue Pan,[1,2] Wenxin Jia,[1,2] Yingsheng Gao,[1,2] Yufei Zhang,[1,2] Nan Zhang,[5] Yinan Zhang,[5] Quan Zhang,[6] Dalei Wu,[7] Chengjie Shan,[8] Meiling Zhang,[8] Bernd Schnabl,[9] Song Yang,[10,§] Xu Shen,[3,§] and Lirui Wang[1,2,§]

[1]*School of Basic Medicine and Clinical Pharmacy, State Key Laboratory of Natural Medicines, China Pharmaceutical University, Nanjing, China;* [2]*Institute of Modern Biology, Nanjing University, Nanjing, China;* [3]*School of Medicine and Holistic Integrative Medicine, Nanjing University of Chinese Medicine, Nanjing, China;* [4]*Department of Gastroenterology, Sir Run Run Hospital, Nanjing Medical University, Nanjing, China;* [5]*Jiangsu Key Laboratory for Functional Substances of Chinese Medicine, School of Pharmacy, Nanjing University of Chinese Medicine, Nanjing, China;* [6]*Institute of Comparative Medicine, College of Veterinary Medicine, Yangzhou University, Yangzhou, China;* [7]*Helmholtz International Lab, State Key Laboratory of Microbial Technology, Shandong University, Qingdao, China;* [8]*School of Life Sciences, East China Normal University, Shanghai, China;* [9]*Department of Medicine, University of California San Diego, La Jolla, California;* [10]*Department of Hepatology, Beijing Ditan Hospital, Capital Medical University, Beijing, China*

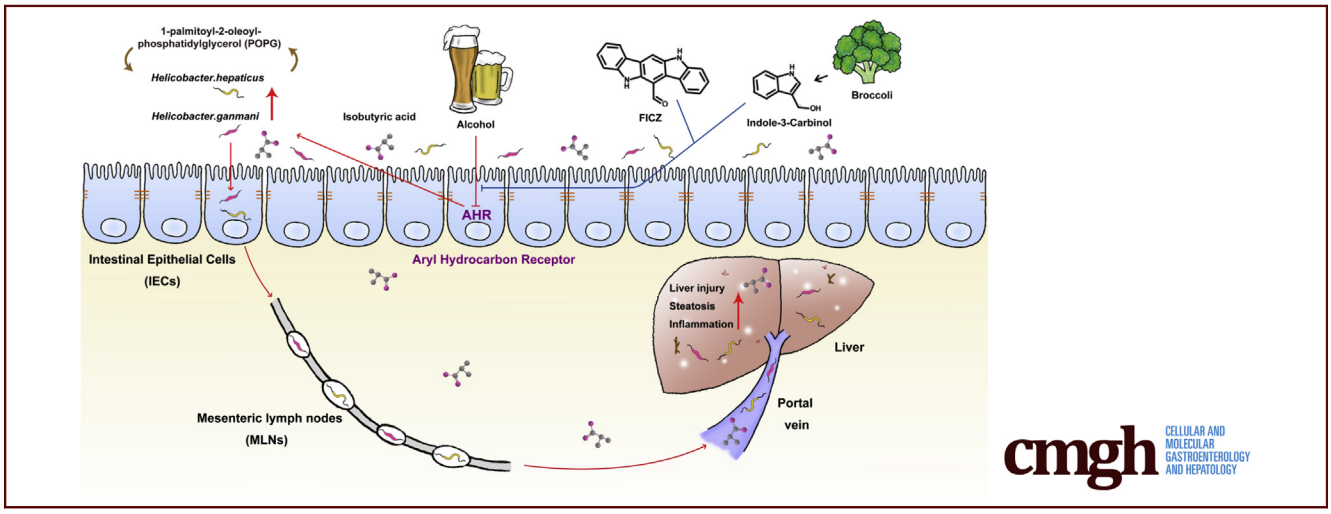

SUMMARY

Herein, we identified that *Ahr* deficiency in intestinal epithelial cells enriched *Helicobacter hepaticus* and *Helicobacter ganmani* in the gut, promoted their translocation to liver, and aggravated alcohol-related liver disease (ALD) development. Dietary supplementation with AHR agonists effectively ameliorated ALD in mice, providing a new strategy for ALD treatment.

BACKGROUND & AIMS: The ligand-activated transcription factor, aryl hydrocarbon receptor (AHR) can sense xenobiotics, dietary, microbial, and metabolic cues. Roles of *Ahr* in intestinal epithelial cells (IECs) have been much less elucidated compared with those in intestinal innate immune cells. Here, we explored whether the IEC intrinsic *Ahr* could modulate the development of alcohol-related liver disease (ALD) via the gut–liver axis.

METHODS: Mice with IEC specific *Ahr* deficiency ($Ahr^{\Delta IEC}$) were generated and fed with a control or ethanol diet. Alterations of intestinal microbiota and metabolites were investigated by 16S ribosomal RNA sequencing, metagenomics, and untargeted metabolomics. AHR agonists were used to evaluate the therapeutic potentials of intestinal *Ahr* activation for ALD treatment.

RESULTS: $Ahr^{\Delta IEC}$ mice showed more severe liver injury after ethanol feeding than control mice. *Ahr* deficiency in IECs altered the intestinal metabolite composition, creating an environment that promoted the overgrowth of *Helicobacter hepaticus* and *Helicobacter ganmani* in the gut, enhancing their translocation to mesenteric lymph nodes and liver. Among the altered metabolites, isobutyric acid was increased in the cecum of ethanol-fed $Ahr^{\Delta IEC}$ mice relative to control mice. Furthermore, both *H. hepaticus* and isobutyric acid administration aggravated ethanol-induced liver injury in vivo and in vitro. Supplementation with AHR agonists, 6-formylindolo[3,2-b] carbazole and indole-3-carbinol, protected mice from ALD

development by specifically activating intestinal *Ahr* without affecting liver *Ahr* function. Alcoholic patients showed lower intestinal AHR expression and higher *H. hepaticus* levels compared with healthy individuals.

CONCLUSIONS: Our results indicate that targeted restoration of IEC intrinsic *Ahr* function may present as a novel approach for ALD treatment. *(Cell Mol Gastroenterol Hepatol 2022;13:233–256; https://doi.org/10.1016/j.jcmgh.2021.08.014)*

Keywords: Aryl Hydrocarbon Receptor; Alcohol-Related Liver Disease; *Helicobacter hepaticus*; Isobutyric Acid.

Alcohol-related liver disease (ALD) is a leading cause of liver-related morbidity and mortality worldwide, and approximately 2 million people die of liver diseases each year, of which up to 50% mortality from cirrhosis can be attributed to alcohol.[1,2] Over the past 25 years, adult per capita alcohol consumption increased by 10%.[3] The exact mechanisms underpinning the pathogenesis of ALD remain unclear. Therefore, elucidating the mechanism and exploring novel therapies for ALD urgently are needed given that the current treatments are very scarce.[1–4]

Aryl hydrocarbon receptor (*Ahr*) is a highly conserved, ligand-inducible transcription factor that integrates environmental, dietary, microbial, and metabolic cues to control the adaptation of multicellular organisms to environmental challenges.[5,6] The *Ahr* is expressed in many mammalian tissues, especially in the liver, intestine, and kidney.[7] In the intestine, *Ahr* is expressed mainly by epithelial cells and innate immune cells, and plays an important role in the regulation of innate immunity.[6] For example, it regulates the number of intraepithelial lymphocytes,[8] controls the production of interleukin 22 by innate lymphoid cells,[9,10] and senses the bacterial virulence factors then leads to antibacterial responses.[11] Compared with the role of *Ahr* in innate immune cells in the intestine, the function of *Ahr* in intestinal epithelial cells (IECs) has not been studied. One previous study showed that *Ahr* in IECs was associated with maintenance of epithelial barrier function.[12] Given that chronic alcohol consumption can disrupt the intestinal epithelial barrier and alter gut microecology, which contributes to ALD,[13,14] we investigated whether intestinal epithelial *Ahr* affects the progression of ALD.

Gut dysbiosis, which contributes to the pathogenesis of ALD, could present as intestinal barrier dysfunction, gut microbiota alteration, and immune system dysregulation.[14–16] Bacterial components and metabolites translocate from the leaky gut through blood and lymphatics to the liver in animal models and patients with ALD.[14,16,17] Once the microbial products translocate to the liver, they activate the innate immune receptors and induce the increased expression of hepatic inflammatory cytokines and lipogenesis-related factors, which promote the development of ALD.[16–18] Not only bacterial products, but viable microbiota also can translocate to the liver. Using regenerating islet-derived 3 gamma (Reg3g) or Reg3b-deficient mice, we previously showed that the translocation of intestinal mucosa-associated bacteria to mesenteric lymph nodes and the liver could aggravate the progression of ALD.[19] In addition, translocating *Enterococcus* to the liver could increase interleukin 1β secretion via the pathogen-recognition receptor Toll-like receptor 2 in Kupffer cells, resulting in hepatic inflammation and hepatocytes death,[20] while administration of bacteriophages against *Enterococcus faecalis* significantly reduced the severity of ALD in mice.[21] Translocation of gut bacteria to the liver also occurred in other liver diseases such as autoimmune hepatitis.[22] Because the translocation of microbial products and intestinal bacteria play such an important role in the pathogenesis of chronic liver diseases, including ALD, it is quite essential to identify new metabolites and strains of bacteria translocating to the liver, and reveal the pathogenic mechanism by which they affect the development of ALD.

Here, we found that ethanol feeding reduced the intestinal AHR expression in mice and human beings. Compared with $Ahr^{fl/fl}$ mice, IEC-specific *Ahr* deletion mice ($Ahr^{\Delta IEC}$) showed aggravated liver injury after ethanol feeding. And the levels of *Helicobacter hepaticus*, *Helicobacter ganmani*, and isobutyric acid (IBA) were enriched in ethanol-fed $Ahr^{\Delta IEC}$ mice compared with $Ahr^{fl/fl}$ mice. In line with the increase of IBA, bacterial gene expression of *ilvE*, *bkdA*, and *pdhD*, which were responsible for metabolizing valine to IBA, were increased in ethanol-fed $Ahr^{\Delta IEC}$ mice. Further investigation showed that *H. hepaticus* and IBA could aggravate ethanol-induced liver injury in vivo and in vitro. Moreover, oral administration with agonists of AHR, 6-formylindolo[3,2-b]carbazole (FICZ)[10] and indole-3-carbinol (I3C),[5] could improve ethanol-induced liver damage in mice, indicating that *Ahr* in IECs may become a novel target for the treatment of ALD.

Results

Ahr *Deficiency in IECs Aggravates Ethanol-Induced Liver Injury*

We first showed that ethanol (EtOH) feeding mice subjected to the chronic-plus-binge model[23] showed decreased messenger RNA (mRNA) levels of *Ahr* and its downstream target genes (*Cyp1a1*, *Cyp1a2*, and *Cyp1b1*) in IECs (Figure 1*A–D*). Furthermore, ethanol exposure could directly down-regulate *Ahr* expression in the murine

***Authors share co-first authorship; §Authors share co-senior authorship.**

Abbreviations used in this paper: **AHR, aryl hydrocarbon receptor; $Ahr^{fl/fl}$, $Ahr^{flox/flox}$; $Ahr^{\Delta IEC}$, intestinal epithelial cell–specific *Ahr* deficiency; ALD, alcohol-related liver disease; AML12, alpha mouse liver 12; ALT, alanine aminotransferase; DMSO, dimethyl sulfoxide; FFA, fatty acid; FICZ, 6-formylindolo[3,2-b]carbazole; I3C, indole-3-carbinol; IBA, isobutyric acid; IEC, intestinal epithelial cell; LEfSe, linear discriminant analysis effect size; MLN, mesenteric lymph node; mRNA, messenger RNA; OD_{600}, optical density analysis at 600 nm; PBS, phosphate-buffered saline; POPG, 1-palmitoyl-2-oleoyl-phosphatidylglycerol; qPCR, quantitative polymerase chain reaction; rRNA, ribosomal RNA; SCFA, short-chain fatty acid; TG, triglyceride; WT, wild-type.**

Most current article

© 2021 The Authors. Published by Elsevier Inc. on behalf of the AGA Institute. This is an open access article under the CC BY-NC-ND license (http://creativecommons.org/licenses/by-nc-nd/4.0/).

2352-345X
https://doi.org/10.1016/j.jcmgh.2021.08.014

intestine-derived epithelial cell line (MODE-K) (Figure 1*E*). To explore the effects of *Ahr* deficiency on the progression of alcohol-related liver disease (ALD), the $Ahr^{\Delta IEC}$ mice were generated and validated by quantitative polymerase chain reaction (qPCR) and immunohistochemical staining (Figure 1*F* and *G*). Although body weight and food intake did not show significant differences between $Ahr^{fl/fl}$ and $Ahr^{\Delta IEC}$ mice after control or ethanol feeding (Figure 1*H* and *I*), $Ahr^{\Delta IEC}$ mice developed more severe liver injury and steatosis relative to $Ahr^{fl/fl}$ mice after ethanol feeding as shown by the increased plasma alanine aminotransferase (ALT) level, H&E staining of liver sections, Oil red O staining of liver sections, and the higher hepatic triglyceride level (Figure 1*J*–*N*). After ethanol administration, livers of $Ahr^{\Delta IEC}$ mice also showed significantly higher mRNA expression of inflammation-related genes, including *Il1b*, *Il6*, *Cxcl5*, and *Cxcl10*, as compared with control mice (Figure 1*O*). However, we found that the hepatic mRNA levels of *Tnf*, *Adgre1* (also known as F4/80), and *Ly6g* in EtOH-fed $Ahr^{\Delta IEC}$ mice were comparable with those in $Ahr^{fl/fl}$ mice (Figure 1*P*). Consistently, hepatic myeloperoxidase + neutrophils and tumor necrosis factor α protein expression in $Ahr^{\Delta IEC}$ mice did not differ from $Ahr^{fl/fl}$ mice after alcohol feeding (Figure 1*Q* and *R*). To further clarify the crucial genes contributing to the increased lipid accumulation in ethanol-fed $Ahr^{\Delta IEC}$ mice, we evaluated the hepatic expression of genes involved in free fatty acids (FFAs) and triglyceride (TG) synthesis, elongation, and hydrolysis. Among these, we found that the expression of elongation of very long chain fatty acid protein 7 (*Elovl7*), which encodes an enzyme that is responsible for the elongation of FFAs, was increased nearly 5-fold in the livers of $Ahr^{\Delta IEC}$ mice than that in $Ahr^{fl/fl}$ mice after ethanol administration (Figure 1*O* and *P*), suggestive of its potential role in promoting lipogenesis in $Ahr^{\Delta IEC}$ mice.

To examine whether *Ahr* deficiency in IECs affects the absorption and metabolism of ethanol, we determined the level of ethanol in plasma and metabolism of ethanol in livers. The plasma ethanol level did not differ significantly between $Ahr^{fl/fl}$ and $Ahr^{\Delta IEC}$ mice after ethanol feeding (Figure 2*A*), and the hepatic gene expression of *Adh1* and *Cyp2e1* (the 2 main primary enzymes that convert ethanol to acetaldehyde)[24,25] were comparable between ethanol-fed $Ahr^{fl/fl}$ and $Ahr^{\Delta IEC}$ mice (Figure 2*B* and *C*). These results indicate that *Ahr* deficiency in IECs promoted ethanol-induced liver disease without affecting intestinal absorption and hepatic metabolism of ethanol in mice.

Ahr *Deficiency in IECs Promotes Translocation of* H. hepaticus *and* H. ganmani *to Liver in Mice*

Increasing evidence has shown that intestinal microbiota dysbiosis has been implicated in the progression of ALD,[14–16] we thus used 16S ribosomal RNA (rRNA) gene sequencing to investigate the effects of IEC-specific *Ahr* disruption on gut microbiota. As shown by the principal coordinate analysis plot, we showed that the composition of intestinal microbiota in ethanol-fed mice clustered separately from that of pair-fed control mice (Figure 3*A*), while the overall microbiota composition of $Ahr^{\Delta IEC}$ mice did not differ significantly from $Ahr^{fl/fl}$ mice either on a control or ethanol diet (Figure 3*A*). Despite that the total number of intestinal bacteria remained unchanged between ethanol-fed $Ahr^{fl/fl}$ and $Ahr^{\Delta IEC}$ mice (Figure 3*B*), the cladogram (linear discriminant analysis effect size [LEfSe] analysis) showed that the abundance of *Helicobacter* (the family level is Helicobacteraceae, the order level is Campylobacterales) was enriched (linear discriminant analysis score > 2) in ethanol-fed $Ahr^{\Delta IEC}$ mice compared with $Ahr^{fl/fl}$ mice (Figure 3*Ci*, C*j*, C*k*, and *D*). *Helicobacter* also was increased slightly ($P = 0.076$) in control-fed $Ahr^{\Delta IEC}$ mice in comparison with $Ahr^{fl/fl}$ mice (Figure 3*E*). *Alistipes* (the family level is *Rikenellaceae*) was found to be enriched in the cecal content of EtOH-fed $Ahr^{\Delta IEC}$ mice as evidenced by the 16S rRNA sequencing results (Figure 3*C* and *D*), although this increase could not be confirmed using a qPCR assay (Figure 3*F*). In addition, the 3 main species of *Alistipes*, including *Alistipes finegoldii*, *Alistipes timonensis*, and *Alistipes indistinctus*, did not alter significantly between ethanol-fed $Ahr^{fl/fl}$ and $Ahr^{\Delta IEC}$ mice (Figure 3*F*).

Furthermore, we also confirmed that the species of *H. hepaticus* and *H. ganmani* (2 species of *Helicobacter*) were increased in the cecum content of ethanol-fed $Ahr^{\Delta IEC}$ mice relative to $Ahr^{fl/fl}$ mice as determined by qPCR (Figure 3*G*). Accordingly, ethanol-fed $Ahr^{\Delta IEC}$ mice showed significantly higher levels of *H. hepaticus* and *H. ganmani* both in mesenteric lymph nodes (MLNs) and livers compared with the ethanol-fed $Ahr^{fl/fl}$ mice (Figure 3*H* and *I*), indicating that IEC-specific *Ahr* deficiency might facilitate the translocation of *H. hepaticus* and *H. ganmani* from the gut to liver after ethanol exposure. In addition, we also showed that levels of most commonly studied bacteria such as *Enterococcus*, *Bifidobacterium*, *Clostridium*, and *Prevotella* did not change obviously in livers between EtOH-fed $Ahr^{fl/fl}$ and $Ahr^{\Delta IEC}$ mice, although Firmicutes (phylum) and *Enterococcus* (genus) were increased in MLNs of $Ahr^{\Delta IEC}$ mice (Figure 3*J*).

More importantly, we found that the relative level of *H. hepaticus* in cecum was correlated positively with hepatic steatosis, *Il6*, and *Cxcl5*, but not *Il1b* and *Cxcl10* expression (Figure 3*K* and *L*). Notably, the gene expression of gut barrier function–related proteins such as occludin (*Ocln*), tight junction protein 1 (*Tjp1*), *Tjp2*, and mucin 2 (*Muc2*) were reduced dramatically in the distal small intestine of $Ahr^{\Delta IEC}$ mice relative to $Ahr^{fl/fl}$ mice after ethanol feeding (Figure 4*A*). Consistently, lipopolysaccharide levels in plasma also were increased significantly in ethanol-fed $Ahr^{\Delta IEC}$ mice compared with $Ahr^{fl/fl}$ mice (Figure 4*B*), suggesting that *Ahr* deficiency in IECs disrupted intestinal epithelial barrier function. Of note, we failed to detect the higher mRNA levels of stem cell markers (*Lrig1* and *Lgr5*) in the intestine of ethanol-fed $Ahr^{\Delta IEC}$ mice, although previous study showed that *Ahr* deletion in IECs promoted stem cell proliferation upon injury of infection or chemical insults,[12] the gene expression of *Il22* and *Il17* in the proximal small intestine did not show the obvious difference either between ethanol-fed $Ahr^{\Delta IEC}$ and $Ahr^{fl/fl}$ mice

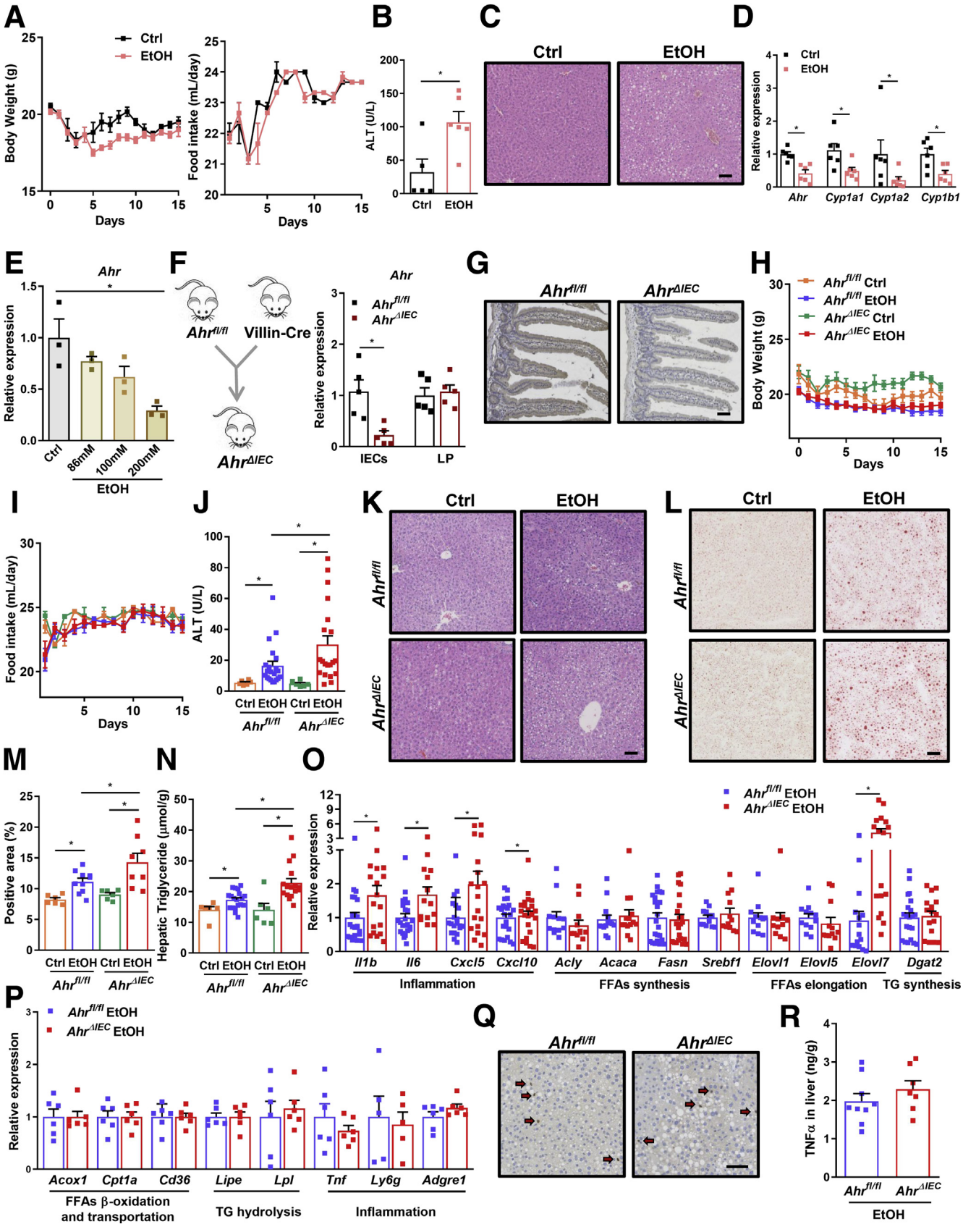
A
Body Weight (g)
Ctrl
EtOH
Days
Food intake (mL/day)
B
ALT (U/L)
C
Ctrl
EtOH
D
Relative expression
Ahr
Cyp1a1
Cyp1a2
Cyp1b1
E
Ahr
Relative expression
Ctrl
86mM
100mM
200mM
EtOH
F
Ahr^fl/fl
Villin-Cre
Ahr^ΔIEC
IECs
LP
G
Ahr^fl/fl
Ahr^ΔIEC
H
Ahr^fl/fl Ctrl
Ahr^fl/fl EtOH
Ahr^ΔIEC Ctrl
Ahr^ΔIEC EtOH
Body Weight (g)
Days
I
Food intake (mL/day)
J
ALT (U/L)
K
L
M
Positive area (%)
N
Hepatic Triglyceride (μmol/g)
O
Relative expression
Il1b
Il6
Cxcl5
Cxcl10
Acly
Acaca
Fasn
Srebf1
Elovl1
Elovl5
Elovl7
Dgat2
Inflammation
FFAs synthesis
FFAs elongation
TG synthesis
P
Acox1
Cpt1a
Cd36
Lipe
Lpl
Tnf
Ly6g
Adgre1
FFAs β-oxidation and transportation
TG hydrolysis
Inflammation
Q
R
TNFα in liver (ng/g)

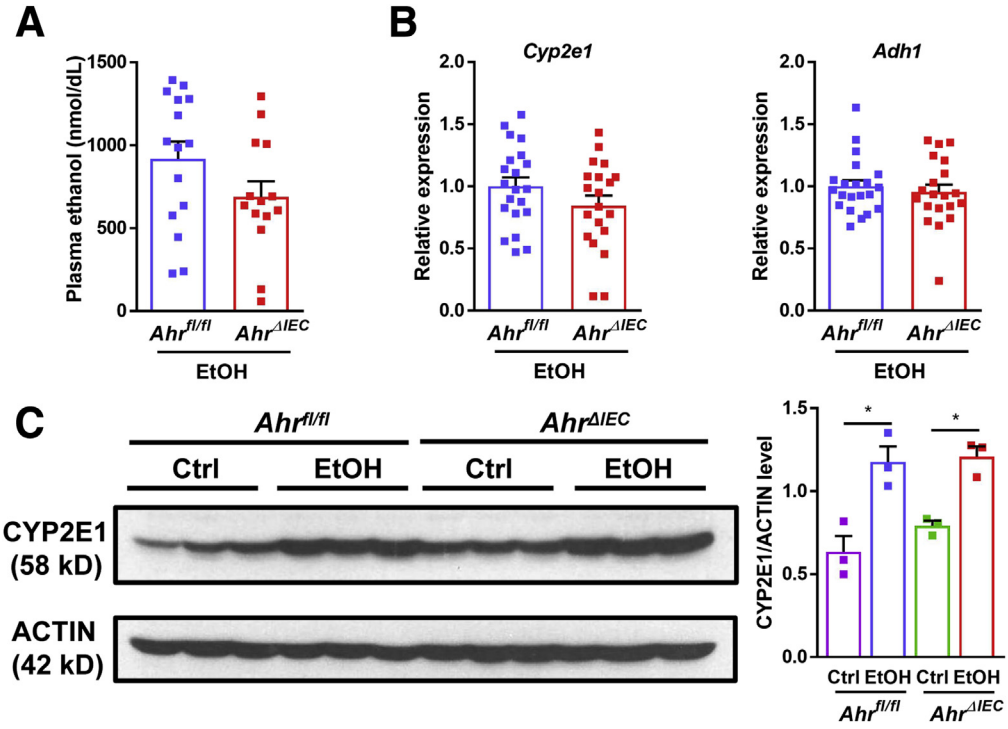

Figure 2. *Ahr* deficiency in IECs causes the progression of ethanol-induced liver damage independent of ethanol absorption and metabolism. (*A*) Plasma ethanol level (n = 15 for $Ahr^{fl/fl}$; n = 14 for $Ahr^{\Delta IEC}$) and (*B*) hepatic mRNAs of *Cyp2e1* and *Adh1* in $Ahr^{fl/fl}$ and $Ahr^{\Delta IEC}$ mice fed an ethanol diet (n = 21 for $Ahr^{fl/fl}$; n = 20 for $Ahr^{\Delta IEC}$). (*C*) Western blot of hepatic CYP2E1 and its quantification (n = 3 per group). Data are represented as means ± SEM. *$P < 0.05$, unpaired *t* test. Ctrl, control.

([Figure 4C](#)).[26] Taken together, *Ahr* deficiency in IECs enriched intestinal *Helicobacter* and aggravated their translocation to liver, eventually leading to enhanced alcohol-related liver injury.

IEC-Specific Ahr *Deficiency Up-regulates IBA Level in the Intestines of Mice*

To further decipher the underlying mechanism that IEC-specific *Ahr* deficiency promotes ethanol-induced liver damage, we also used untargeted metabolomics to assess the alteration of cecum metabolites between ethanol-fed $Ahr^{fl/fl}$ and $Ahr^{\Delta IEC}$ mice. The top 20 Kyoto Encyclopedia of Genes and Genomes (KEGG) pathways with significant differences are shown in [Figure 5A](#), and pathways such as protein digestion and absorption, aminoacyl-tRNA biosynthesis, and mineral absorption differed extensively between ethanol-fed $Ahr^{\Delta IEC}$ and control mice. Although the tryptophan level was reduced in ethanol-fed $Ahr^{\Delta IEC}$ mice, the level of kynurenic acid, which was converted from kynurenine, a main metabolite of tryptophan, was comparable between $Ahr^{fl/fl}$ and $Ahr^{\Delta IEC}$ mice ([Figure 5B](#)). Indole and its derivatives, microbe-dependent products of tryptophan, did not alter dramatically either in these 2 groups of mice ([Figure 5B](#)). Instead, 64 metabolites with significant change were identified, among them, IBA, a short-chain fatty acid (SCFA), was increased notably in ethanol-fed $Ahr^{\Delta IEC}$ mice compared with control mice ([Figure 5C–E](#)). The other SCFAs, including acetic acid, propionic acid, and butyric acid, were not different between the ethanol-fed $Ahr^{\Delta IEC}$ mice and the $Ahr^{fl/fl}$ mice ([Figure 5F](#)). More importantly, we found that the increased level of IBA was correlated positively with hepatic steatosis and expression of inflammation-related genes ([Figure 5G and H](#)). Consistent with the increase of

Figure 1. (*See previous page*). *Ahr* deficiency in IECs of mice exacerbates ethanol-induced liver injury. (*A–D*) WT mice were fed a control or ethanol diet (n = 5–6 per group). (*A*) Body weight and food intake. (*B*) Plasma level of ALT. (*C*) Representative H&E staining images of liver sections. (*D*) qPCR analysis of *Ahr*, *Cyp1a1*, *Cyp1a2*, and *Cyp1b1* in IECs isolated from control (Ctrl) and ethanol-fed mice subjected to the chronic-plus-binge model (n = 6 per group). (*E*) mRNA expression analysis of *Ahr* in murine intestine-derived epithelial cell (MODE-K) stimulated with ethanol (n = 3 independent experiments performed in 2 replicates). (*F*) Schematic of $Ahr^{\Delta IEC}$ mice and the qPCR analysis of *Ahr* in IECs and lamina propria (LP) cells (n = 5 per group). (*G*) Representative images of immunohistochemical staining for AHR expression in small intestine of $Ahr^{fl/fl}$ and $Ahr^{\Delta IEC}$ mice. (*H–N*) $Ahr^{fl/fl}$ and $Ahr^{\Delta IEC}$ mice were fed a control or ethanol diet. (*H*) Body weight and (*I*) food intake (n = 6 for Ctrl; n = 22–23 for EtOH). (*J*) Plasma level of ALT (n = 6 for Ctrl; n = 20–21 for EtOH). (*K*) Representative H&E staining images of liver sections. (*L* and *M*) Representative Oil red O–stained liver sections quantified by Image J (n = 5–6 for Ctrl; n = 8–10 for EtOH). (*N*) Hepatic TG content (n = 6 for Ctrl; n = 16–19 for EtOH). (*O*) Hepatic expression of mRNA encoded by inflammation, FFAs, and TG synthesis-related genes in ethanol-fed $Ahr^{fl/fl}$ and $Ahr^{\Delta IEC}$ mice (n = 12–23). (*P*) Hepatic expression of mRNA in ethanol-fed $Ahr^{fl/fl}$ and $Ahr^{\Delta IEC}$ mice (n = 6 per group). (*Q*) Myeloperoxidase staining of liver sections from ethanol-fed $Ahr^{fl/fl}$ and $Ahr^{\Delta IEC}$ mice (n = 7–9). (*R*) Hepatic expression of tumor necrosis factor (TNF)α protein (n = 7–9). *Scale bar*: 50 μm. Data are represented as means ± SEM. *$P < 0.05$, (*J* and *N*) Mann–Whitney test; (*A, B, D, E, F, H, I, M, O, P* and *R*) unpaired *t* test.

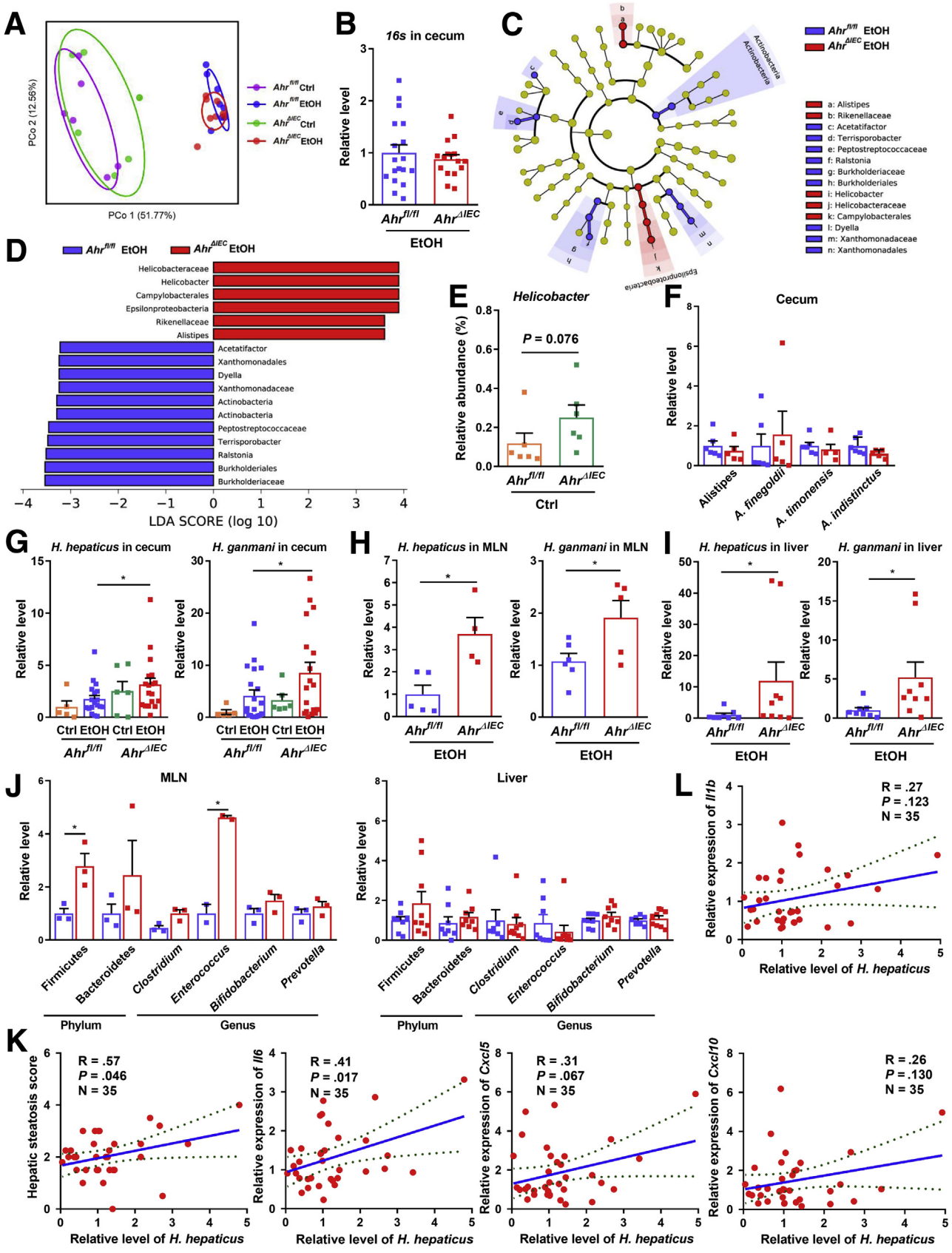
A
PCo 2 (12.56%)
PCo 1 (51.77%)
Ahr fl/fl Ctrl
Ahr fl/fl EtOH
Ahr ΔIEC Ctrl
Ahr ΔIEC EtOH
B
16s in cecum
Relative level
Ahr fl/fl
Ahr ΔIEC
EtOH
C
Actinobacteria
Epsilonproteobacteria
Ahr fl/fl EtOH
Ahr ΔIEC EtOH
a: Alistipes
b: Rikenellaceae
c: Acetatifactor
d: Terrisporobacter
e: Peptostreptococcaceae
f: Ralstonia
g: Burkholderiaceae
h: Burkholderiales
i: Helicobacter
j: Helicobacteraceae
k: Campylobacterales
l: Dyella
m: Xanthomonadaceae
n: Xanthomonadales
D
Ahr fl/fl EtOH
Ahr ΔIEC EtOH
Helicobacteraceae
Helicobacter
Campylobacterales
Epsilonproteobacteria
Rikenellaceae
Alistipes
Acetatifactor
Xanthomonadales
Dyella
Xanthomonadaceae
Actinobacteria
Actinobacteria
Peptostreptococcaceae
Terrisporobacter
Ralstonia
Burkholderiales
Burkholderiaceae
LDA SCORE (log 10)
E
Helicobacter
Relative abundance (%)
P = 0.076
Ahr fl/fl
Ahr ΔIEC
Ctrl
F
Cecum
Relative level
Alistipes
A. finegoldii
A. timonensis
A. indistinctus
G
H. hepaticus in cecum
H. ganmani in cecum
Relative level
Ctrl EtOH Ctrl EtOH
Ahr fl/fl
Ahr ΔIEC
H
H. hepaticus in MLN
H. ganmani in MLN
Relative level
Ahr fl/fl
Ahr ΔIEC
EtOH
I
H. hepaticus in liver
H. ganmani in liver
Relative level
Ahr fl/fl
Ahr ΔIEC
EtOH
J
MLN
Liver
Relative level
Firmicutes
Bacteroidetes
Clostridium
Enterococcus
Bifidobacterium
Prevotella
Phylum
Genus
L
Relative expression of Il1b
R = .27
P = .123
N = 35
Relative level of H. hepaticus
K
Hepatic steatosis score
R = .57
P = .046
N = 35
Relative level of H. hepaticus
Relative expression of Il6
R = .41
P = .017
N = 35
Relative level of H. hepaticus
Relative expression of Cxcl5
R = .31
P = .067
N = 35
Relative level of H. hepaticus
Relative expression of Cxcl10
R = .26
P = .130
N = 35
Relative level of H. hepaticus

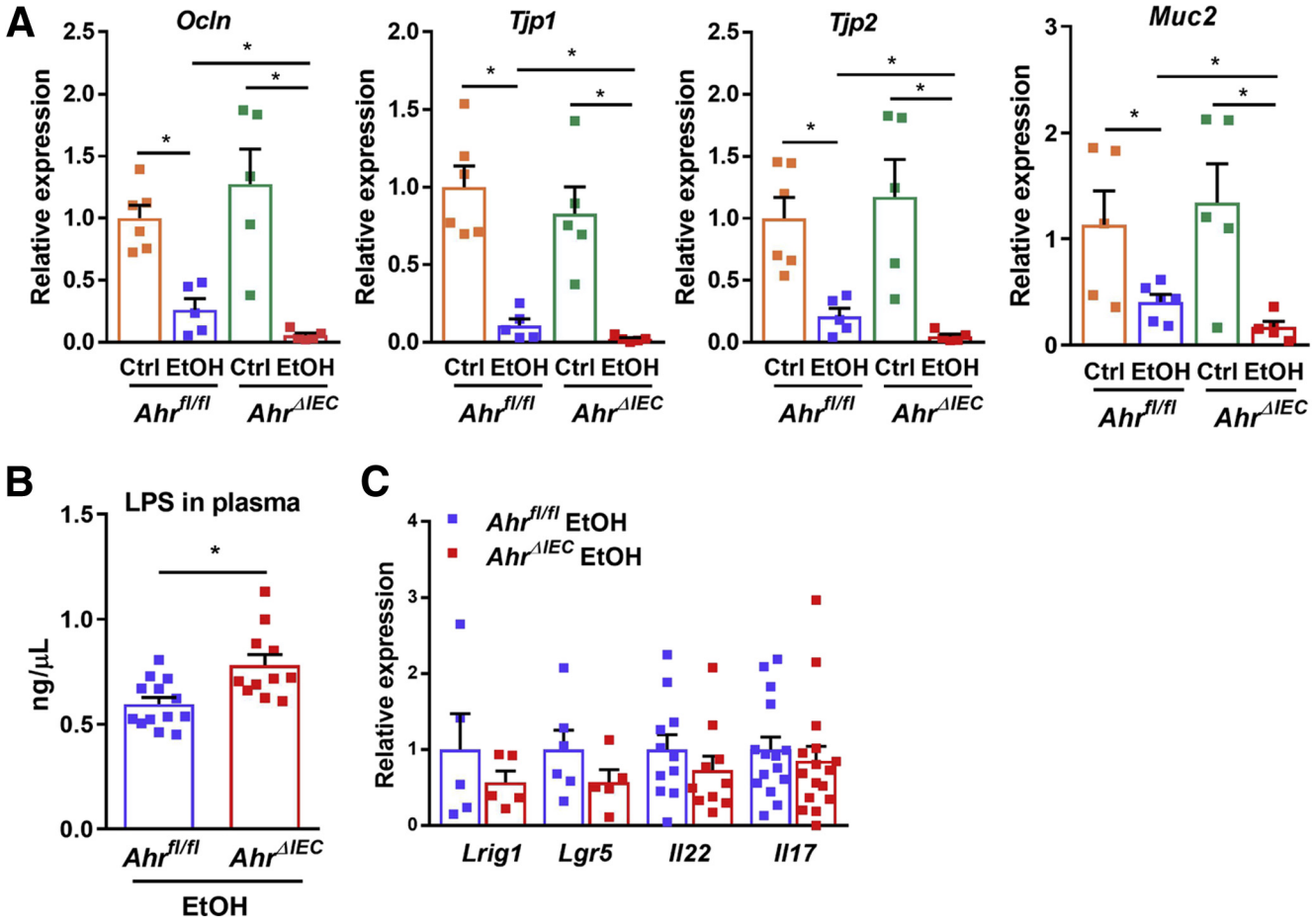

Figure 4. *Ahr* deficiency in IECs disrupted the intestinal epithelial barrier. (*A*) mRNA levels of *Ocln*, *Tjp1*, *Tjp2*, and *Muc2* in the distal small intestine (n = 5–6 per group). (*B*) Plasma level of lipopolysaccharide (LPS) in EtOH-fed $Ahr^{fl/fl}$ and $Ahr^{\Delta IEC}$ mice (n = 13 for $Ahr^{fl/fl}$; n = 11 for $Ahr^{\Delta IEC}$). (*C*) mRNA levels of leucine-rich repeats and immunoglobulin-like domains 1 (*Lrig1*), leucine-rich repeat containing G-protein–coupled receptor 5 (*Lgr5*), *Il22*, and *Il17* in the proximal small intestine of ethanol-fed $Ahr^{fl/fl}$ and $Ahr^{\Delta IEC}$ mice (n = 5–16), *Lrig1* and *Lgr5* are the stem cell markers. Data are represented as means ± SEM. *$P < 0.05$, unpaired *t* test. Ctrl, control.

IBA, shotgun metagenomics analysis showed that the bacterial gene expression of *ilvE, bkdA,* and *pdhD,* which were responsible for metabolizing valine to produce IBA, were increased in the cecum of ethanol-fed $Ahr^{\Delta IEC}$ mice relative to control mice (Figure 5*I* and *J*). Accordingly, we observed the reduction of valine level in these ethanol-fed $Ahr^{\Delta IEC}$ mice (Figure 5*C–E*). To explore whether alterations of gut metabolites were associated with enrichment of *Helicobacter,* we performed a correlation analysis between the 64 altered metabolites and the intestinal abundance of *H. hepaticus* or *H. ganmani*. The anionic phospholipid 1-palmitoyl-2-oleoyl-phosphatidylglycerol (POPG), the

Figure 3. (*See previous page*). *Ahr* deficiency in IECs promotes expansion of cecal *H. hepaticus* and its translocation to the liver in ethanol-induced mice. (*A*) Principal coordinate analysis (PCoA) plot of cecal microbiota of $Ahr^{fl/fl}$ and $Ahr^{\Delta IEC}$ mice fed a control or ethanol diet (n = 6 for control [Ctrl]; n = 8 for EtOH). (*B*) Total bacteria in cecum of ethanol-fed mice (n = 18 for $Ahr^{fl/fl}$; n = 16 for $Ahr^{\Delta IEC}$). (*C*) The cladogram of gut microbiome in different taxonomic levels from ethanol-fed mice. The taxa of different abundance in $Ahr^{fl/fl}$ and $Ahr^{\Delta IEC}$ group are presented in blue and red, respectively (n = 8 per group). (*D*) Significantly altered bacterial taxa between ethanol-fed $Ahr^{fl/fl}$ and $Ahr^{\Delta IEC}$ mice (linear discriminant analysis [LDA] score, >2 or <-2). (*E*) The relative abundance of *Helicobacter* in cecum from control-fed mice detected by 16S rRNA gene sequencing (n = 6 per group). (*F*) The relative levels of *Alistipes* and the 3 main species of *Alistipes* in cecum from EtOH-fed $Ahr^{fl/fl}$ and $Ahr^{\Delta IEC}$ mice determined by qPCR (n = 6 for $Ahr^{fl/fl}$; n = 5 for $Ahr^{\Delta IEC}$). (*G*) The relative level of *H. hepaticus* and *H. ganmani* in cecum from control or ethanol-fed mice (n = 5–6 for Ctrl; n = 18–20 for EtOH) determined by qPCR. (*H* and *I*) *H. hepaticus* and *H. ganmani* in MLNs (n = 4–6 per group) and liver (n = 8–9 per group) of ethanol-fed $Ahr^{fl/fl}$ and $Ahr^{\Delta IEC}$ mice. (*J*) The relative levels of bacteria in MLNs and livers of EtOH-fed mice detected by qPCR (n = 3 per group for MLN; n = 7–9 for liver). (*K*) Correlation analysis between relative level of intestinal *H. hepaticus* with hepatic steatosis (*left panel*), *Il6* (*middle panel*), and *Cxcl5* expression (*right panel*). (*L*) Correlation analysis between the relative level of intestinal *H. hepaticus* with hepatic *Il1b* (*upper*) and *Cxcl10* (*lower*) expression. Data are represented as means ± SEM. *$P < 0.05$, unpaired *t* test.

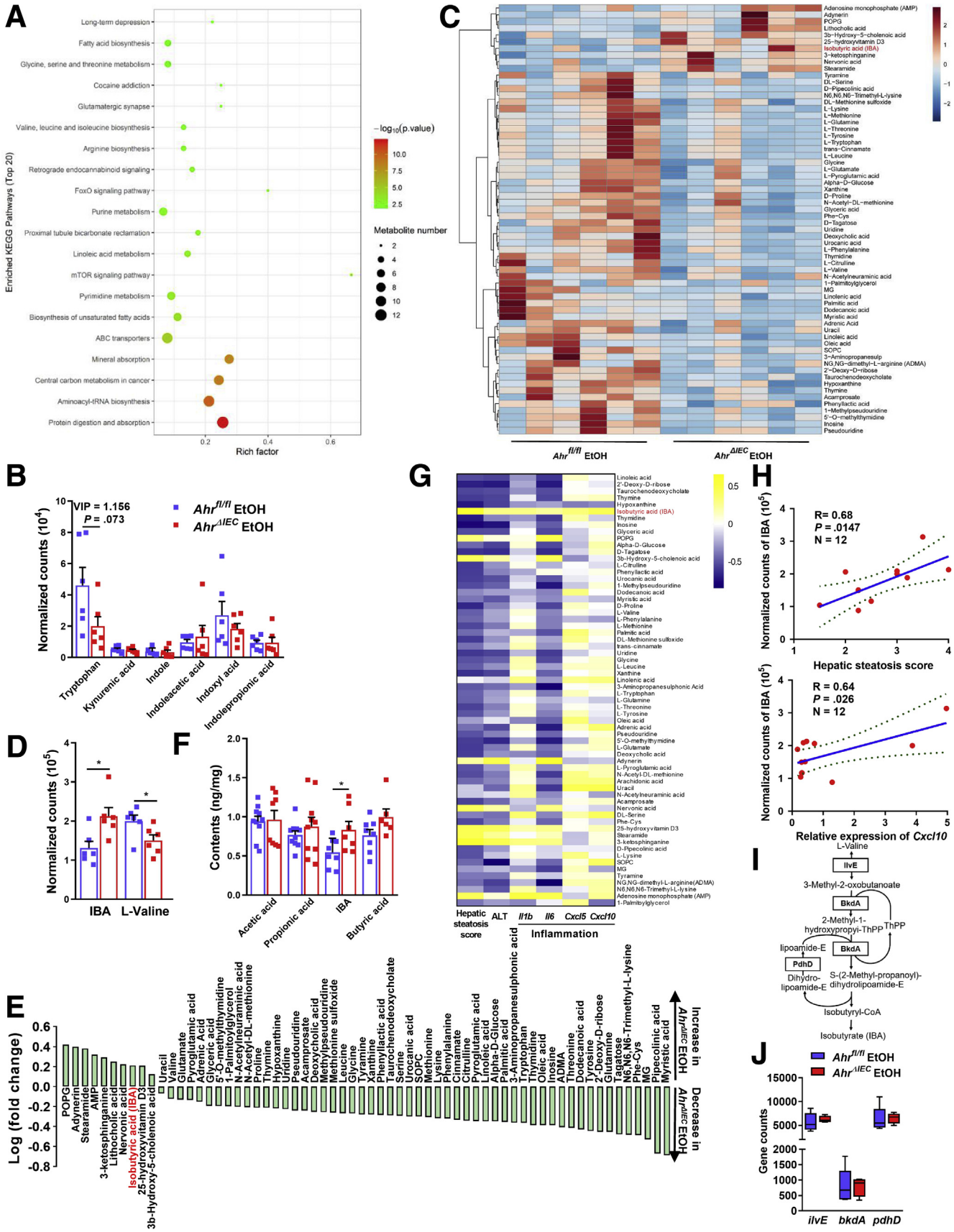
A
Long-term depression
Fatty acid biosynthesis
Glycine, serine and threonine metabolism
Cocaine addiction
Glutamatergic synapse
Valine, leucine and isoleucine biosynthesis
Arginine biosynthesis
Retrograde endocannabinoid signaling
FoxO signaling pathway
Purine metabolism
Proximal tubule bicarbonate reclamation
Linoleic acid metabolism
mTOR signaling pathway
Pyrimidine metabolism
Biosynthesis of unsaturated fatty acids
ABC transporters
Mineral absorption
Central carbon metabolism in cancer
Aminoacyl-tRNA biosynthesis
Protein digestion and absorption
Enriched KEGG Pathways (Top 20)
Rich factor
−log10(p.value)
Metabolite number
B
VIP = 1.156
P = .073
Ahr fl/fl EtOH
Ahr ΔIEC EtOH
Normalized counts (10^4)
Tryptophan
Kynurenic acid
Indole
Indoleacetic acid
Indoxyl acid
Indolepropionic acid
C
Ahr fl/fl EtOH
Ahr ΔIEC EtOH
D
Normalized counts (10^5)
IBA
L-Valine
F
Contents (ng/mg)
Acetic acid
Propionic acid
IBA
Butyric acid
G
Hepatic steatosis score
ALT
Il1b
Il6
Cxcl5
Cxcl10
Inflammation
H
R= 0.68
P = .0147
N = 12
Normalized counts of IBA (10^5)
Hepatic steatosis score
R = 0.64
P = .026
N = 12
Relative expression of Cxcl10
I
L-Valine
IlvE
3-Methyl-2-oxobutanoate
BkdA
2-Methyl-1-hydroxypropyl-ThPP
ThPP
lipoamide-E
BkdA
PdhD
Dihydro-lipoamide-E
S-(2-Methyl-propanoyl)-dihydrolipoamide-E
Isobutyryl-CoA
Isobutyrate (IBA)
J
Ahr fl/fl EtOH
Ahr ΔIEC EtOH
Gene counts
ilvE
bkdA
pdhD
E
Log (fold change)
Increase in Ahr ΔIEC EtOH
Decrease in Ahr ΔIEC EtOH

secondary bile acid lithocholic acid, which was reported to cause liver injury,[27] nervonic acid, and the stearamide, which was increased in patients with alcoholic cirrhosis,[28] showed significant positive correlations with the abundance of *H. hepaticus* (Figure 6*A* and *B*), while the other 4 metabolites including hypoxanthine, phenylalanine-cysteine, acamprosate, and thymine showed negative correlations with *H. hepaticus* (Figure 6*C*). In addition, we found that metabolites such as adynerin, POPG, and adenosine monophosphate were correlated positively with *H. ganmani*, while linoleic acid was correlated negatively with *H. ganmani* (Figure 6*D* and *E*).

Subsequently, we evaluated the effects of the correlated metabolites on the growth of *H. hepaticus* in vitro. We found that only the lipid POPG could significantly promote the growth of *H. hepaticus* (Figure 6*F*). Interestingly, the untargeted metabolomics analysis showed that *H. hepaticus* per se could produce POPG as the metabolite (Figure 6*G*), although we cannot exclude that POPG also possibly was derived from the host. Consistently, the intestinal POPG level in mice fed with *H. hepaticus* also was higher than that in control mice (Figure 6*H*). More importantly, we also showed that POPG could enhance *H. hepaticus* growth in intestinal organoids (Figure 6*I* and *J* and Supplementary Video). Therefore, we provided mechanistic evidence that POPG might be the most important metabolite to promote the enrichment of *H. hepaticus* in the intestine.

H. hepaticus *Aggravates Ethanol-Induced Injury In Vivo and In Vitro*

To further prove that the IEC-specific *Ahr* deficiency–induced increase of *H. hepaticus* promotes the development of ALD, we challenged wild-type (WT) mice with *H. hepaticus* every other day in a chronic-plus-binge model. *H. hepaticus* administration markedly increased levels of *H. hepaticus* (>500-fold) in feces of mice (Figure 7*A*). In line with this, mice gavaged with *H. hepaticus* developed more severe ethanol-induced hepatic injury, indicated by increased ALT level (Figure 7*B*), increased hepatic steatosis (Figure 7*C*), as well as enhancement of hepatic *Cxcl5* and *Cxcl10* expression (Figure 7*D*). Consistently, both cultured hepatocytes and Kupffer cells stimulated with *H. hepaticus* in vitro recapitulated the effects of *H. hepaticus* in vivo. *H. hepaticus*–treated mouse hepatocyte alpha mouse liver 12 (AML12) cells showed more lipid droplet accumulation (Figure 7*E* and *F*) and increased expression of inflammation-related genes such as *Il1b*, *Il6*, *Cxcl5*, and *Cxcl10* in either basal or ethanol-stimulated conditions (Figure 7*G*). Notably, *H. hepaticus*–induced increment of *Cxcl10* expression became more obvious in the presence of ethanol (Figure 7*G*). In addition, *H. hepaticus* also could induce the increase of *Il1b*, *Il6*, *Cxcl5*, and *Cxcl10* gene expression in Kupffer cells (Figure 7*H*), which is comparable with that in hepatocytes. These results provided direct evidence that *H. hepaticus* could aggravate liver injury in vivo and in vitro.

IBA Induces Liver Injury in Mice and Cultured Hepatocytes

IBA level was increased in ethanol-fed $Ahr^{\Delta IEC}$ mice compared with $Ahr^{fl/fl}$ mice (Figure 5*C*), we thus investigated whether the increased IBA also could contribute to the progression of ALD. Administration of IBA in C57BL/6 mice showed obvious liver damage as indicated by the increased plasma ALT level, hepatic lipid accumulation, and higher hepatic TG level compared with control mice (Figure 8*A*–*C*). We also noticed that IBA could significantly increase hepatic *Cxcl5* gene expression (Figure 8*D*). Consistent with this, AML12 cells stimulated with IBA showed more lipid accumulation and increased gene expression of hepatic *Cxcl5* and *Cxcl10* (Figure 8*E*–*G*). Similarly, IBA also could increase *Cxcl5* and *Cxcl10* expression in Kupffer cells (Figure 8*H*). More interestingly, we found that *H. hepaticus* could boost the effects of IBA on lipid accumulation (Figure 8*I* and *J*). It should be noted that IBA treatment alone or in combination with ethanol significantly up-regulated *Elovl7* expression in AML12 cells (Figure 8*K*), which is consistent with the increased *Elovl7* expression in ethanol-fed $Ahr^{\Delta IEC}$ mice, which had the higher level of IBA in vivo (Figures 1*O* and 5*C*–*F*). We thus sought to determine the effect of *Elovl7* on lipid accumulation in hepatocytes. Overexpression of *Elovl7* resulted in more lipid droplet accumulation in AML12 cells, either in basal or alcohol-stimulated conditions (Figure 8*L* and *M*). All of these results showed that IBA could induce hepatic steatosis and liver damage in vivo and in vitro, while *H. hepaticus* was able to enhance the effects of IBA on lipogenesis. We

Figure 5. (*See previous page*). *Ahr* deficiency in IECs increases intestinal IBA. (*A*) The Kyoto Encyclopedia of Genes and Genomes (KEGG) enrichment analysis of intestinal metabolites from ethanol-fed $Ahr^{fl/fl}$ and $Ahr^{\Delta IEC}$ mice (n = 6 per group). (*B*) Tryptophan, kynurenic acid, indole, indoleacetic acid, indoxyl acid, and indolepropionic acid levels in cecum of ethanol-fed $Ahr^{fl/fl}$ and $Ahr^{\Delta IEC}$ mice (n = 6 per group). (*C*) The heatmap of the relative abundance of each significantly altered metabolite in cecum between ethanol-fed $Ahr^{fl/fl}$ and $Ahr^{\Delta IEC}$ mice (n = 6 per group), 64 metabolites were identified with significant alteration (variable influence on projection [VIP] > 1.0; $P < 0.1$). (*D*) IBA and valine levels in the cecum content of ethanol-fed $Ahr^{fl/fl}$ and $Ahr^{\Delta IEC}$ mice (n = 6 per group). (*E*) Identification of 64 metabolites with a significant increase (upward) or decrease (downward) in ethanol-fed $Ahr^{\Delta IEC}$ mice compared with $Ahr^{fl/fl}$ mice. (*F*) Cecal contents of SCFAs in ethanol-fed $Ahr^{fl/fl}$ and $Ahr^{\Delta IEC}$ mice (n = 7–10). (*G*) Spearman correlation of the 64 metabolites with hepatic steatosis score, ALT level, and inflammation. (*H*) Pearson correlation of hepatic steatosis score, *Cxcl10* with intestinal IBA level. (*I*) Scheme for IBA-synthesis pathway. *IlvE*, branched-chain amino acid aminotransferase (EC:2.6.1.42); *BkdA*, 2-oxoisovalerate dehydrogenase E1 component (EC:1.2.4.4); and *PdhD*, dihydrolipoamide dehydrogenase (EC:1.8.1.4). (*J*) The counts of the genes involved in the IBA-synthesis pathway, including *ilvE*, *bkdA*, and *pdhD*, analyzed by shotgun metagenomics. n = 5 for $Ahr^{fl/fl}$; n = 4 for $Ahr^{\Delta IEC}$. Data are represented as means ± SEM. *$P < 0.05$, unpaired *t* test.

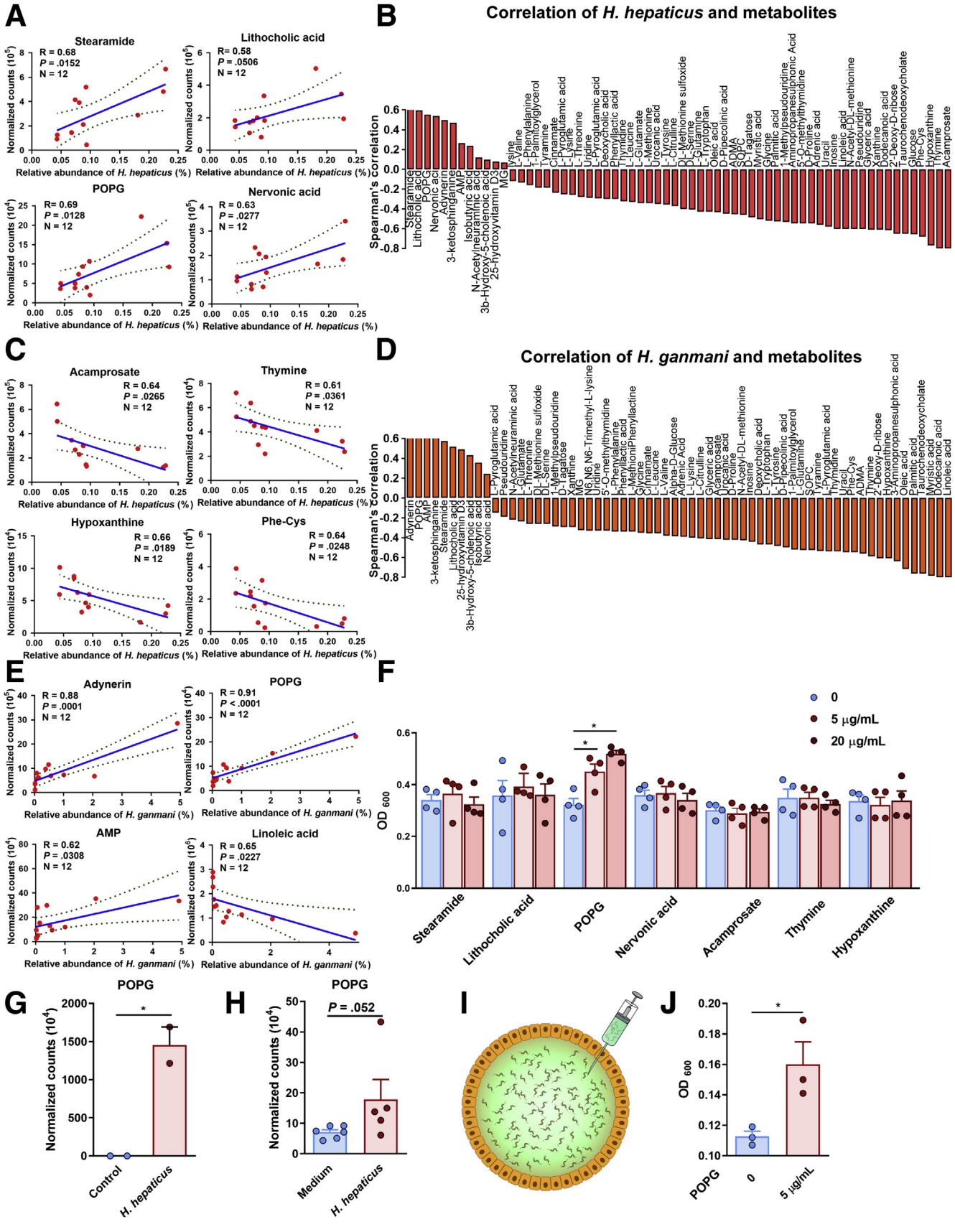
A
Stearamide
R = 0.68
P = .0152
N = 12
Lithocholic acid
R= 0.58
P = .0506
N = 12
POPG
R= 0.69
P = .0128
N = 12
Nervonic acid
R = 0.63
P = .0277
N = 12
Normalized counts (10^5)
Normalized counts (10^4)
Relative abundance of H. hepaticus (%)
B
Correlation of H. hepaticus and metabolites
Spearman's correlation
Stearamide
Lithocholic acid
POPG
Nervonic acid
3-ketosphinganine
Adynerin
AMP
Isobutyric acid
N-Acetylneuraminic acid
3b-Hydroxy-5-cholenoic acid
25-hydroxyvitamin D3
MG
Lysine
L-Valine
L-Phenylalanine
1-Palmitoylglycerol
Tyramine
Cinnamate
L-Glutamic acid
L-Lysine
L-Threonine
Uridine
L-Pyroglutamic acid
Deoxycholic acid
Phenylacetic acid
L-Leucine
L-Glutamate
L-Methionine
Urocanic acid
L-Tyrosine
L-Citrulline
DL-Methionine sulfoxide
DL-Serine
L-Tryptophan
Oleic acid
Glyceric acid
Adrenic Acid
SOPC
D-Tagatose
Myristic acid
Glycine
Palmitic acid
Pseudouridine
Amiloxatepanesulphonic Acid
5'-O-methylthymidine
D-Proline
Adrenic acid
Uracil
Taurine
Linoleic acid
N-Acetyl-DL-methionine
Pseudouridine
Gluconic acid
Xanthine
2'-Deoxy-D-ribose
Taurochenodeoxycholate
Glucose
Phe-Cys
Hypoxanthine
Thymine
Acamprosate
C
Acamprosate
R = 0.64
P = .0265
N = 12
Thymine
R = 0.61
P = .0361
N = 12
Hypoxanthine
R = 0.66
P = .0189
N = 12
Phe-Cys
R = 0.64
P = .0248
N = 12
Relative abundance of H. hepaticus (%)
D
Correlation of H. ganmani and metabolites
Spearman's correlation
Adynerin
POPG
AMP
3-ketosphinganine
Stearamide
Lithocholic acid
25-hydroxyvitamin D3
3b-Hydroxy-5-cholenoic acid
Isobutyric acid
Nervonic acid
L-Pyroglutamic acid
Pseudouridine
N-Acetylneuraminic acid
Uridine
L-Threonine
DL-Methionine sulfoxide
DL-Serine
5'-O-methylthymidine
Phenylacetic acid
L-Methionine
Phenyllactine
Glycine
Cinnamate
L-Leucine
L-Valine
Adrenic Acid
Alpha-D-Glucose
L-Lysine
L-Citrulline
Glyceric acid
Acamprosate
Urocanic acid
N-Acetyl-DL-methionine
Inosine
Deoxycholic acid
L-Tryptophan
L-Tyrosine
Linoleic acid
1-Palmitoylglycerol
L-Glutamine
SOPC
Tyramine
L-Pyroglutamic acid
Thymidine
Phe-Cys
ADMA
Thymine
2'-Deoxy-D-ribose
Hypoxanthine
Arachidonoyl ethanolamine
Oleic acid
Palmitic acid
Taurochenodeoxycholate
Myristic acid
Dodecanoic acid
Linoleic acid
E
Adynerin
R = 0.88
P = .0001
N = 12
POPG
R = 0.91
P < .0001
N = 12
AMP
R = 0.62
P = .0308
N = 12
Linoleic acid
R = 0.65
P = .0227
N = 12
Relative abundance of H. ganmani (%)
F
0
5 μg/mL
20 μg/mL
OD 600
Stearamide
Lithocholic acid
POPG
Nervonic acid
Acamprosate
Thymine
Hypoxanthine
G
POPG
Normalized counts (10^4)
Control
H. hepaticus
H
POPG
P = .052
Normalized counts (10^4)
Medium
H. hepaticus
I
J
OD 600
POPG
0
5 μg/mL

also elucidated the crucial role of *Elovl7* in IBA-induced lipid accumulation.

AHR Agonists Ameliorate ALD in Mice

Two widely used agonists for AHR, I3C and FICZ,[12,29] whose activation effects on *Ahr* were confirmed in vitro by ourselves (Figure 9*A* and *B*), were selected to explore whether supplementation with AHR agonists could be a therapeutic approach for ALD. WT mice exposed to an ethanol diet were orally gavaged with I3C (50 mg/kg) and FICZ (50 μg/kg) daily for 15 days. Although body weight and food intake showed no significant differences compared with control mice (Figure 9*C*), both I3C and FICZ decreased hepatic steatosis (Figure 9*D*), decreased liver TG levels (Figure 9*E*), and reduced mRNA expression of *Elovl7*, *Il6*, *Cxcl5*, and *Cxcl10* (Figure 9*F* and *G*). Subsequently, we confirmed that I3C and FICZ activated AHR in the intestine as shown by the increased gene expression of *Cyp1a1* and *Cyp1b1* (Figure 9*H*), whereas they did not activate hepatic AHR (Figure 9*I*), suggesting that selectively activating intestinal AHR was sufficient to protect mice from alcohol-induced liver damage. Intriguingly, mice treated with I3C and FICZ dramatically decreased the abundance of intestinal *H. hepaticus* (Figure 9*J*). Collectively, our findings show the therapeutic potentials of AHR agonists for ALD treatment.

Alcoholic Patients Showed Decreased Intestinal AHR Expression and Increased H. hepaticus Level

To explore whether the decreased intestinal AHR expression was relevant to alcoholic patients, we analyzed their levels in the duodenal tissues. As expected, the mRNA and protein expression of intestinal AHR was decreased significantly in alcoholic patients compared with nonalcoholic individuals by qPCR analysis and immunohistochemical staining (Figure 10*A* and *B*). Intriguingly, compared with healthy controls, patients with alcoholic liver disease showed a higher level of fecal *H. hepaticus* (Figure 10*C*). Notably, 1 patient with an alcohol-use history for more than 30 years (2–3 bottles of liquor for daily drinking, equal to 400–600 g pure alcohol/d) and very severe aspartate aminotransferase, γ-glutamyl transferase, and Fibrosis-4 index levels, had a remarkably higher abundance of *H. hepaticus* in the stool sample (Figure 10*C*).

Discussion

Ahr is widely expressed throughout the body, and intestinal *Ahr* was reported to play an important role in enteric diseases such as inflammatory bowel disease and colitis by regulation of the immune response and intestinal barrier functions.[6,8,12] However, the association between intestinal *Ahr* and liver diseases still remains largely unexplored. The AHR ligands constitute a large family that generally can be categorized into 4 major sources: xenobiotics (eg, dioxin), dietary metabolites (eg, I3C), endogenous metabolites (eg, indole acetic acid), and microbial derivatives (eg, indirubin).[30,31] Although ethanol is not identified as a direct ligand of AHR, ethanol feeding was shown to reduce microbiota-dependent AHR ligand production from tryptophan in mice such as indole acetic acid.[26] Notably, AHR activation by microbial tryptophan metabolites were shown to improve ALD in mice,[32] highlighting the association of ALD with intestinal AHR and microbiota. We thus attempt to explore the crosstalk between intestinal AHR and gut microbiota, as well as their metabolites, and clarify the role of intestinal AHR in the progression of ALD.

Considering that IECs function as the first line sensing intestinal environment change derived from dietary, microbial, and metabolic cues, we generated IEC-specific *Ahr*-deficiency mice in which *Ahr* expression in lamina propria cells remained unchanged. We showed that *Ahr* depletion in IECs did not directly affect intestinal absorption and metabolism of ethanol. In addition, we could not find that a lack of *Ahr* in IECs altered the intestinal mRNA levels of stem cell markers, although 1 previous study showed that *Ahr* deletion in IECs enhanced stem cell proliferation upon injury through infection or chemical insults.[12] The gene expression of *Il22* and *Il17* in the proximal small intestine was not different between ethanol-fed $Ahr^{\Delta IEC}$ mice and control mice.

Here, we observed that alcohol depressed the expression of *Ahr* in IECs in mice and human beings, and its deficiency enhanced the susceptibility to ethanol-induced liver injury.

Figure 6. (*See previous page*). *H. hepaticus* per se could produce POPG as the metabolite that enhances *H. hepaticus* growth. (*A*) The correlation analysis between stearamide, lithocholic acid, POPG, nervonic acid, and the relative abundance of intestinal *H. hepaticus*. (*B*) Spearman rank correlation between significantly altered metabolites and the intestinal relative abundance of *H .hepaticus*. (*C*) The correlation analysis between acamprosate, thymine, hypoxanthine, phenylalanine-cysteine (Phe-Cys) and the relative abundance of intestinal *H. hepaticus*. (*D*) Spearman rank correlation between significantly altered metabolites and the intestinal relative abundance of *H. ganmani*. (*E*) The correlation analysis between adynerin, POPG, adenosine monophosphate (AMP), linoleic acid, and the relative abundance of intestinal *H. ganmani* (Pearson correlation). (*F*) POPG was observed to boost the growth of *H. hepaticus* in vitro. *H. hepaticus* was cultured anaerobically in brucella agar plates containing 8% sheep blood with or without the metabolite for 6 days. Bacteria were collected and suspended in medium and their growth were determined by OD_{600} measurement. n = 4 independent experiments performed in 2 replicates in each experiment. (*G*) The relative level of POPG in control or *H. hepaticus* by untargeted metabolomics (n = 2). (*H*) The level of POPG in the cecal content from mice fed with *H. hepaticus* or broth (n = 5–6). (*I*) Schematic representation of microinjection of *H. hepaticus* into the intestinal organoid. (*J*) POPG enhanced the growth of *H. hepaticus* in the intestinal organoid isolated from WT mice. *H. hepaticus* exposed to POPG or control medium was microinjected into intestinal organoid. After incubation for 4 days in the lumen of the organoid, bacteria were released and cultured anaerobically in brucella agar plates for 6 days and determined by OD_{600} analysis. n = 3 independent experiments performed in 2 replicates in each experiment. Data are represented as means ± SEM. $^*P < 0.05$, unpaired *t* test.

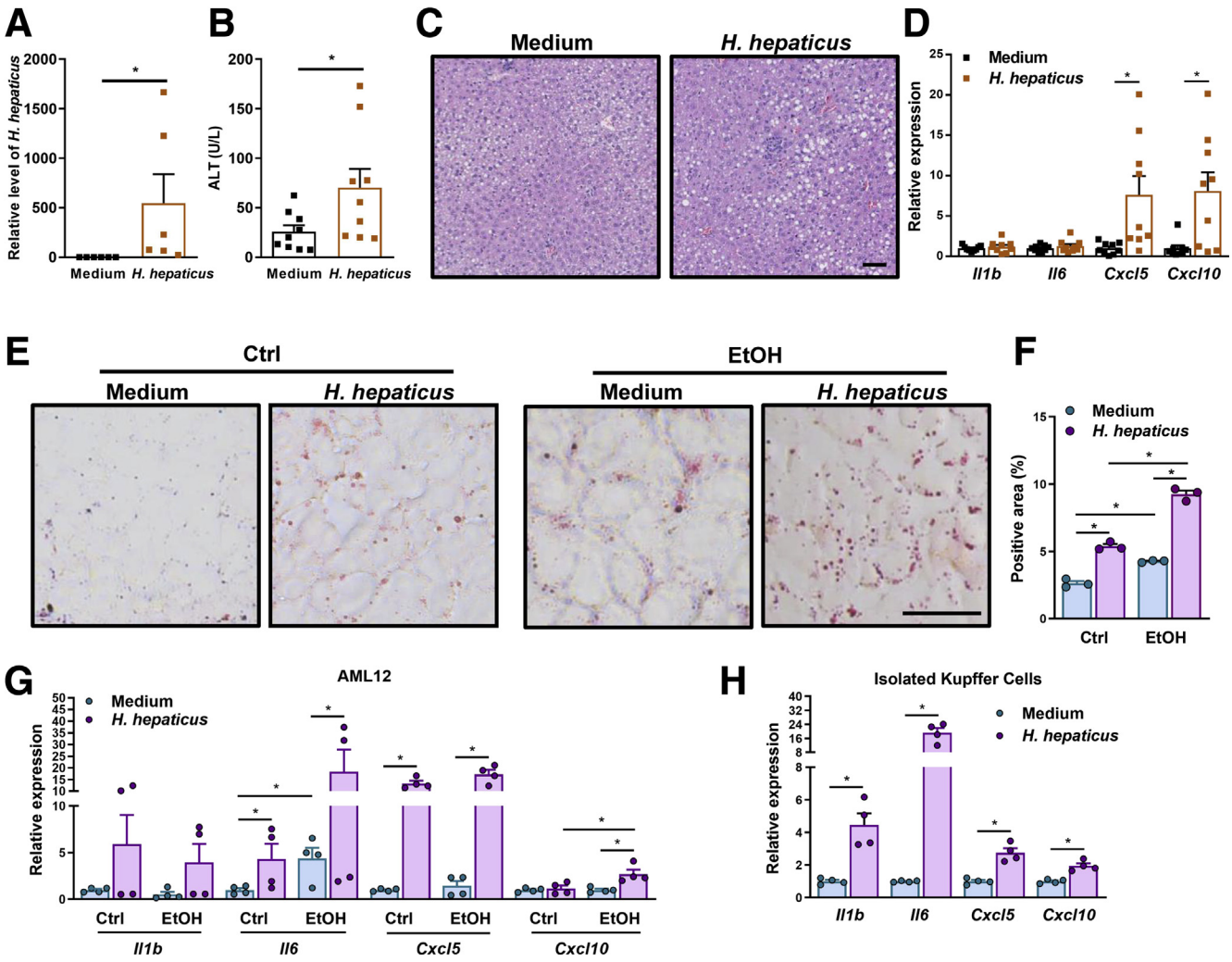

Figure 7. *H. hepaticus* promotes the progression of ALD in vivo and in vitro. (*A–D*) Mice were gavaged with medium or *H. hepaticus* every other day during ethanol feeding. (*A*) Relative level of *H. hepaticus* in the feces of mice administered medium or *H. hepaticus* (n = 6 per group). (*B*) Plasma ALT level (n = 9 per group). (*C*) Representative H&E staining of liver sections (n = 9 per group). (*D*) *Il1b*, *Il6*, *Cxcl5*, and *Cxcl10* mRNA levels in livers (n = 9 per group). (*E–G*) AML12 cells were cultured in plates overnight, and subsequently were stimulated with medium or *H. hepaticus* and exposed to control (Ctrl) or EtOH simultaneously for 24 hours. n = 3–4 independent experiments performed in 2 replicates in each experiment. (*E*) Representative images of Oil red O staining, (*F*) quantified by ImageJ. (*G*) *Il1b*, *Il6*, *Cxcl5*, and *Cxcl10* mRNA levels in AML12 cells. (*H*) *Il1b*, *Il6*, *Cxcl5*, and *Cxcl10* mRNA levels in Kupffer cells stimulated with *H. hepaticus* for 4 hours. n = 4 independent experiments performed in 2 replicates in each experiment. Data are represented as means ± SEM. *$P < 0.05$, (*A*) Mann–Whitney test; (*B, D, F, G* and *H*) unpaired *t* test.

Compared with control mice, intestinal levels of *Helicobacter* (*H. hepaticus* and *H. ganmani*) and IBA were up-regulated in ethanol-fed $Ahr^{\Delta IEC}$ mice, which were accompanied by increased intestinal permeability, and the abundance of *H. hepaticus* and *H. ganmani* in MLNs and liver also were increased accordingly in these mice. Of note, *H. hepaticus* per se could produce POPG as the metabolite that, in turn, enhanced the bacteria growth and promoted its translocation from gut to liver on the basis of the intestinal barrier disruption caused by *Ahr* deficiency. *H. hepaticus* and IBA aggravated ethanol-induced liver injury by eliciting hepatic inflammation and steatosis. Importantly, oral supplementation of AHR agonists FICZ and I3C (a derivative from cruciferous vegetables) markedly ameliorated ALD by activating intestinal *Ahr* and reducing *H. hepaticus* in a mouse model, suggesting a new way for the treatment of ALD (Figure 10*D*). Consistently, a recent study showed that the prebiotic, pectin, could improve alcohol-induced liver injury by increasing the bacterial tryptophan metabolites, and proposed that targeting intestinal AHR activation could improve alcoholic liver disease,[32] however, our study, through using IEC-specific *Ahr*-deficiency mice, showed elaborately that it is the IEC-intrinsic *Ahr* that mediated the beneficial effects of AHR activation on the progression of ALD.

In this study, we showed that a specific dysbiosis, increased intestinal *Helicobacter* species, contributed to the progression of ALD in mice. Previously, *Helicobacter* species

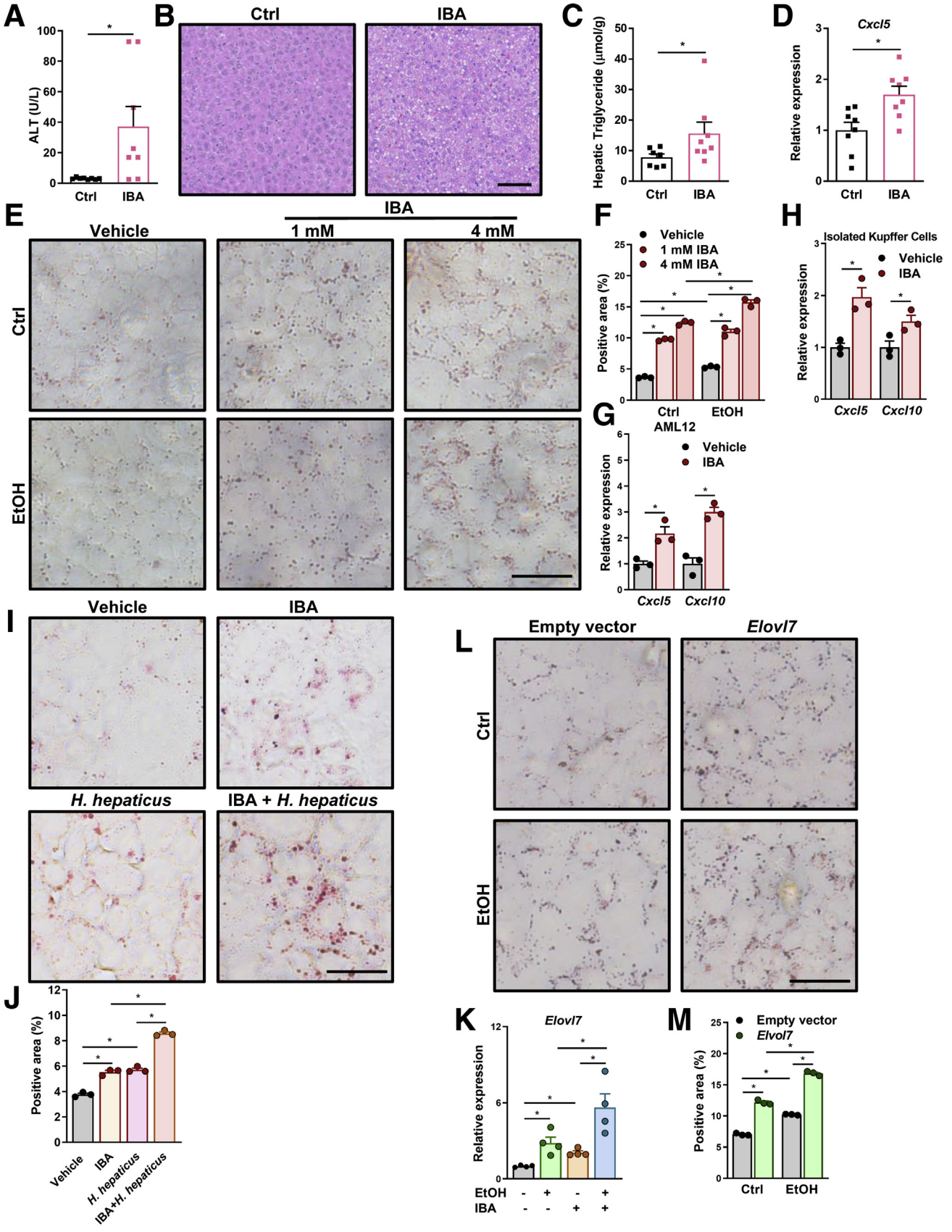
A
ALT (U/L)
Ctrl
IBA
B
Ctrl
IBA
C
Hepatic Triglyceride (μmol/g)
Ctrl
IBA
D
Cxcl5
Relative expression
Ctrl
IBA
E
IBA
Vehicle
1 mM
4 mM
Ctrl
EtOH
F
Vehicle
1 mM IBA
4 mM IBA
Positive area (%)
Ctrl
EtOH
AML12
G
Vehicle
IBA
Relative expression
Cxcl5
Cxcl10
H
Isolated Kupffer Cells
Vehicle
IBA
Relative expression
Cxcl5
Cxcl10
I
Vehicle
IBA
H. hepaticus
IBA + H. hepaticus
J
Positive area (%)
Vehicle
IBA
H. hepaticus
IBA+H. hepaticus
L
Empty vector
Elovl7
Ctrl
EtOH
K
Elovl7
Relative expression
EtOH
IBA
M
Empty vector
Elvol7
Positive area (%)
Ctrl
EtOH

were not regarded as pathogens for human beings because the majority of colonized individuals were asymptomatic.[33] However, increasing evidence has shown a strong association of intestinal *Helicobacter* species with enteric diseases such as Crohn's disease and inflammatory bowel disease in patients, indicating its pathogenicity in the digestive diseases.[34,35] *H. hepaticus*, one of the main species of *Helicobacter*, also could be detected in patients' bile and liver samples, and was associated with chronic liver diseases, including primary hepatocellular carcinoma and bile duct cancer.[36–39] Here, we identified that the *H. hepaticus* level was increased markedly in patients with ALD compared with that in healthy individuals. In addition, *H. ganmani*, another important species of *Helicobacter* with increased abundance in ethanol-induced $Ahr^{\Delta IEC}$ mice, was not explored in this study because of its current unavailability, however, the role of *H. ganmani* in ALD also deserves further investigation.

Besides the changes of gut microbiota, another explanation for the link between gut dysbiosis and liver diseases is the alteration of metabolites produced by the intestinal microbiota. Well-known metabolites such as SCFAs (eg, butyrate, acetate) could exert immunomodulatory effects both inside and outside of the intestine.[40,41] Here, we showed that the SCFA IBA was increased significantly in IEC-specific *Ahr*-deficiency mice compared with control mice after alcohol drinking. Shotgun metagenomics analysis indicated that the pathway contributing to IBA synthesis was more activated in $Ahr^{\Delta IEC}$ mice than that in $Ahr^{fl/fl}$ mice as evidenced by the increased bacterial gene expression of *ilvE*, *bkdA*, and *pdhD*. Notably, the bacterial gene *ilvE*, coding the enzyme responsible for catalyzing valine to 3-methyl-2-oxobutanoate, also could be found in *H. hepaticus*. Thus, we presumed that the increased abundance of *H. hepaticus* in $Ahr^{\Delta IEC}$ mice also may contribute to the increased IBA. Regarding the role of IBA in liver disease, we showed that both IBA administration in vivo and treatment in cultured hepatocytes could induce liver injury when used alone or in combination with alcohol. Although we failed to detect IBA in mice serum, it still is possible that IBA could go to the liver from the portal vein to aggravate the alcohol-induced liver disease in $Ahr^{\Delta IEC}$ mice given that these mice had a disrupted intestinal barrier. Our findings also are consistent with findings in nonalcoholic steatohepatitis patients containing a higher fecal IBA level.[42] These results therefore suggest that fecal IBA might be developed as a new biomarker to predict the progression of ALD.

Mechanistically, we used the combination of 16S rRNA sequencing, metagenomics, and untargeted metabolomics to show that IEC-specific *Ahr* deficiency induced the alteration of intestinal metabolites, these metabolites, such as the anionic phospholipid POPG and the secondary bile acids lithocholic acid, nervonic acid, and stearamide (increased in patients with alcoholic cirrhosis),[28] correlated positively with the abundance of *H. hepaticus*, while metabolites such as hypoxanthine, phenylalanine–cysteine, acamprosate, and thymine correlated negatively with the abundance of *H. hepaticus*. We further showed that the lipid POPG, which was produced by *H. hepaticus*, could in turn promote the growth of the bacteria itself. In addition, acamprosate, a drug for alcohol use disorder treatment,[43,44] was identified as decreased in cecal content from EtOH-fed $Ahr^{\Delta IEC}$ mice by untargeted metabolomics. It showed a negative correlation with *H. hepaticus*, although validation of this metabolite remains to be addressed by targeted metabolomics analysis. All of these changes in metabolite composition might directly promote the overgrowth of intestinal *H. hepaticus*, facilitating its translocation to the liver. At the gene level, we showed that the increased bacterial gene expression of *ilvE*, *bkdA*, and *pdhD* contributed to the increase of IBA in ethanol-fed $Ahr^{\Delta IEC}$ mice relative to control mice, suggesting that these genes might be good targets for regulating the intestinal IBA level. More interestingly, we showed that IBA and *H. hepaticus* could have a synergistic effect on lipogenesis in hepatocytes. Overall, we elucidated the balance of interactions between IEC-intrinsic *Ahr*, gut metabolites, and microbiota, the disruption of this balance came from IEC-specific *Ahr* deficiency, which would lead to the alteration of gut metabolites and microbiota as well as the development of ALD in this study.

Elovl7, one enzyme responsible for the elongation of saturated FFAs, was reported to trigger lipid accumulation in differentiated adipocytes, leading to oxidative damage and inflammation.[45,46] In our study, compared with $Ahr^{fl/fl}$ mice, we found an up-regulated gene expression of hepatic *Elovl7* in ethanol-induced $Ahr^{\Delta IEC}$ mice, which had more severe steatotic livers. This was consistent with the in vitro results that overexpression of *Elovl7* resulted in lipid accumulation in cultured hepatocytes. Mechanistically, we identified that IBA, which was increased in $Ahr^{\Delta IEC}$ mice

Figure 8. (***See previous page***). **IBA induces liver damage in vivo and in vitro.** (*A–D*) Mice were injected intraperitoneally with vehicle or IBA for 24 or 48 hours. (*A*) Plasma ALT level at 24 hours (n = 8 per group). (*B*) Representative H&E staining of liver sections at 48 hours. (*C*) Hepatic TG content (n = 7–8 per group) at 48 hours. (*D*) Hepatic *Cxcl5* mRNA at 24 hours (n = 8 per group). (*E*) AML12 cells were seeded in 12-well plates overnight, and were treated with control (PBS) or ethanol (100 mmol/L), and stimulated with vehicle (DMSO) or IBA (1 and 4 mmol/L) at the same time for 24 hours, and the cells were stained with Oil red O. (*F*) Quantification of the Oil red O staining. (*G* and *H*) mRNA levels of *Cxcl5* and *Cxcl10* in AML12 cells (G) treated with vehicle or IBA for 24 hours and isolated Kupffer cells, or (*H*) treated with vehicle or IBA for 4 hours. n = 3 independent experiments performed in 2 replicates in each experiment. (*I* and *J*) AML12 cells were seeded in 12-well plates overnight and treated with medium, IBA, *H. hepaticus*, and IBA+*H. hepaticus* for 24 hours. The cells were finally stained with Oil red O. (*I*) Representative images of the Oil red O staining. (*J*) Quantification of Oil red O staining. (*K*) *Elovl7* mRNA levels in AML12 cells exposed to EtOH (100 mmol/L), IBA (4 mmol/L), or EtOH (100 mmol/L) + IBA (4 mmol/L). (*L*) Cells were transfected with empty vector or *Elovl7*, and exposed to control or EtOH (100 mmol/L) for 24 hours. Cells were stained with Oil red O. (*M*) Quantification of the Oil red O staining. For cell culture experiments, at least 3 independent experiments were performed with 2 replicates in each experiment. *Scale bar*: 50 μm. Data are represented as means ± SEM. *$P < 0.05$, unpaired *t* test. Ctrl, control.

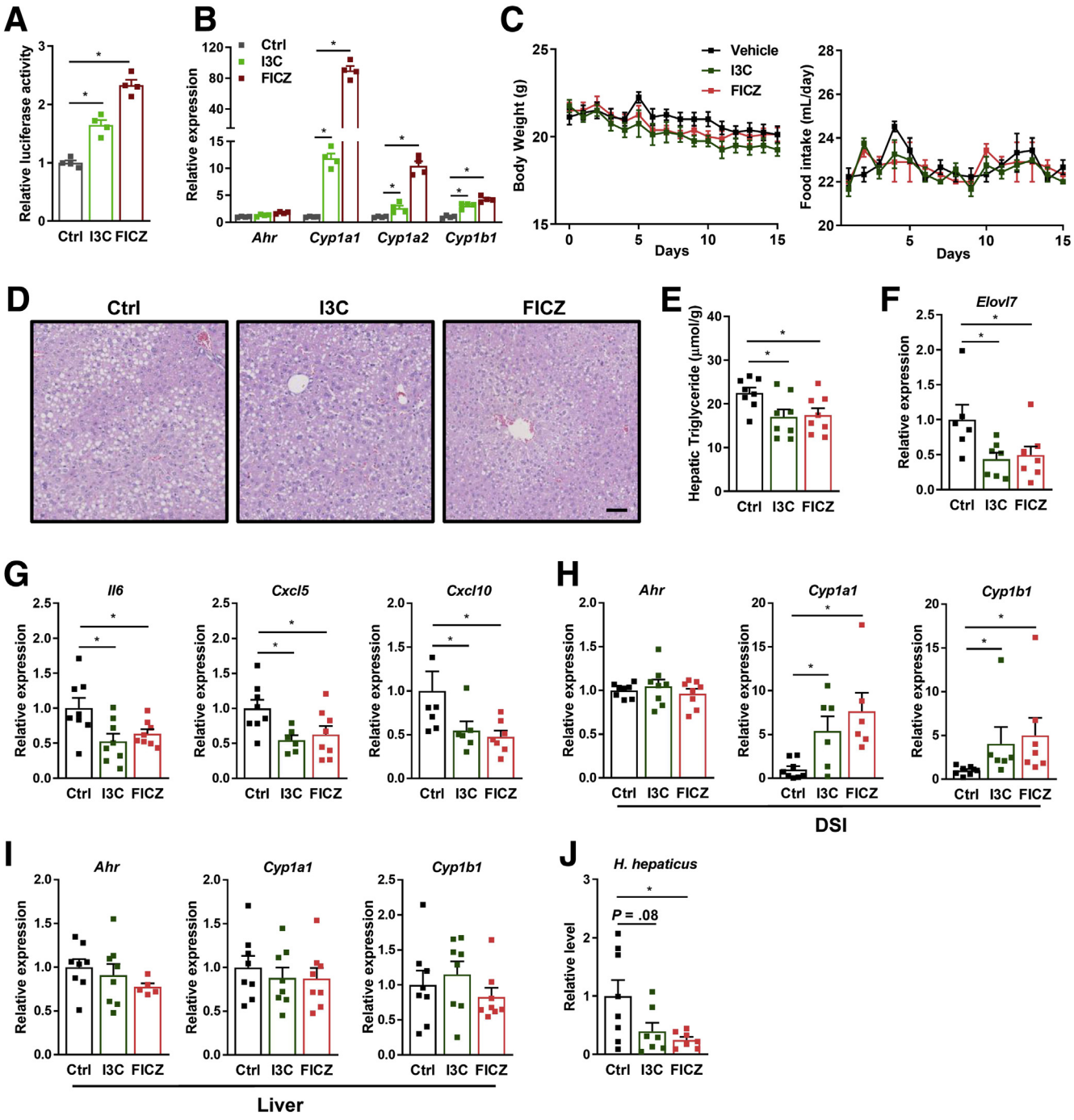

Figure 9. AHR agonists improve ethanol-induced liver disease in mice. (*A*) *Ahr* activation by I3C (50 μmol/L) and FICZ (100 nmol/L) analyzed by luciferase assay (n = 4 independent experiments). (*B*) *Ahr*, *Cyp1a1*, *Cyp1a2*, and *Cyp1b1* mRNA levels in AML12 stimulated with I3C (50 μmol/L) and FICZ (100 nmol/L) (n = 4 independent experiments). (*C–J*) Mice were orally administered vehicle, I3C (50 mg/kg), and FICZ (50 μg/kg), and fed an EtOH diet (n = 6–8 per group). (*C*) Body weight and food intake. (*D*) Representative liver sections stained with H&E. (*E*) Hepatic TG content. (*F*) Hepatic *Elovl7* mRNA level. (*G*) Hepatic *Il6*, *Cxcl5*, and *Cxcl10* mRNA levels. (*H* and *I*) mRNA levels of *Ahr*, *Cyp1a1*, and *Cyp1b1* in distal small intestine and liver. (*J*) The relative level of *H. hepaticus* in cecum. *Scale bar*: 50 μm. Data are represented as means ± SEM. *$P < 0.05$, unpaired *t* test. Ctrl, control.

relative to control mice, could directly up-regulate *Elovl7* mRNA expression in hepatocytes. Our observations thus proved that *Elovl7* might play an important role in regulating hepatic lipid accumulation in the context of alcohol-related liver disease.

In conclusion, we showed an essential role for intestinal epithelial cell intrinsic *Ahr* in regulating hepatic lipid accumulation and inflammation in ALD through affecting *H. hepaticus* and IBA levels, which might serve as predictive biomarkers for the progression of ALD. Moreover, dietary

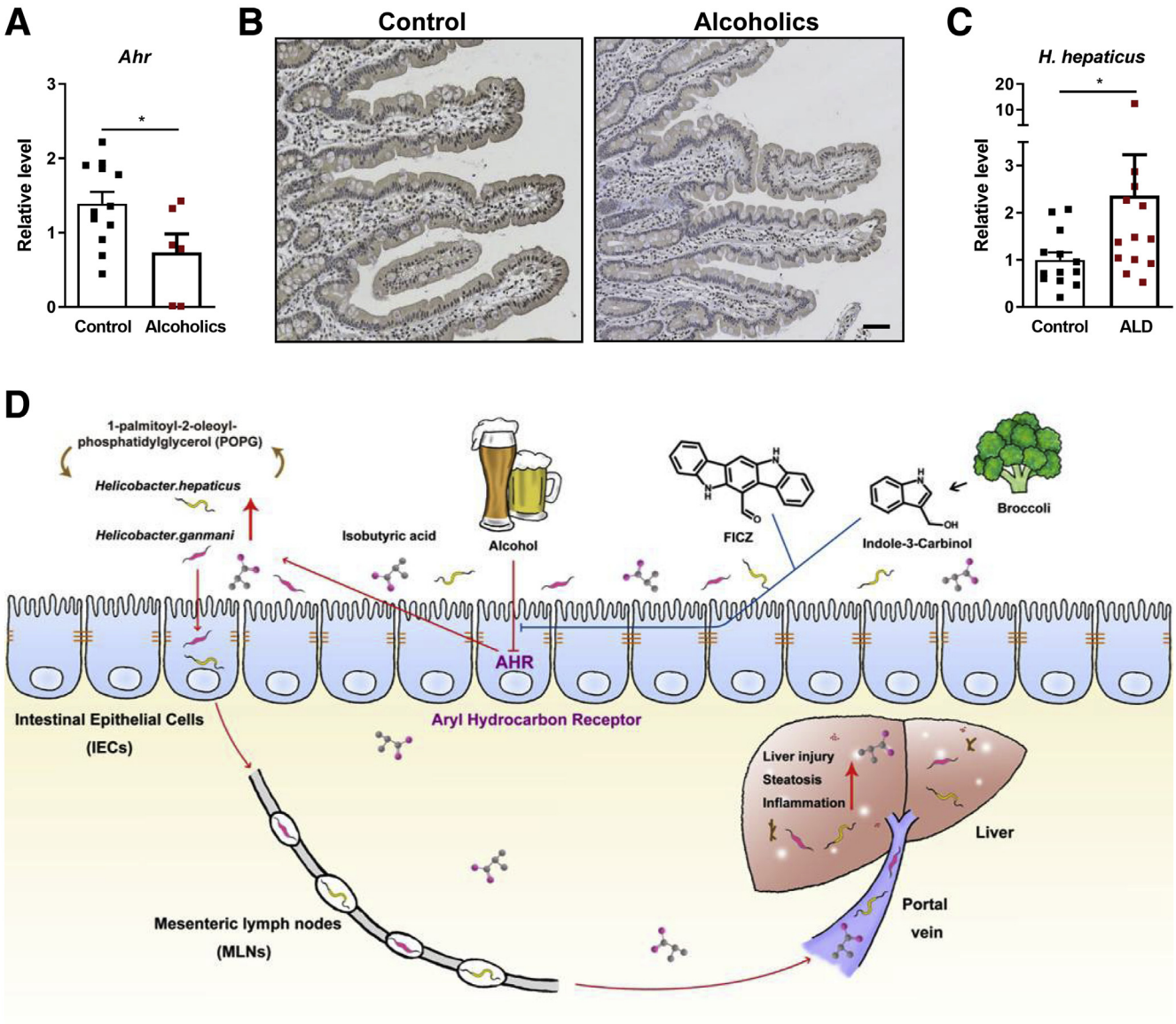

Figure 10. Decreased intestinal AHR level and increased *H. hepaticus* in alcoholic patients. (*A*) mRNA and (*B*) protein levels of AHR in duodenal tissues from controls and alcoholic patients (n = 12 controls; n = 6 alcoholic patients) determined by qPCR and immunohistochemical staining. (*C*) The relative level of *H. hepaticus* in healthy controls and patients with alcoholic liver disease (n = 13 per group). (*D*) A schematic diagram summarizing our findings that alcohol abuse down-regulates AHR expression in IECs, which contributes to ALD progression. Alcohol depresses the expression of *Ahr* in IECs, and subsequently enriches intestinal *H. hepaticus*, *H. ganmani*, and IBA levels. *Ahr* deficiency in IECs exacerbates intestinal *H. hepaticus* and *H. ganmani* translocation through MLNs to liver via the disrupted gut barrier. POPG, 1 metabolite of *H. hepaticus*, in turn boosts *H. hepaticus* growth. *H. hepaticus* and IBA augment ethanol-induced liver injury by eliciting hepatic inflammation and steatosis. Supplementation with AHR agonists, FICZ and indole-3-carbinol (abundant in cruciferous vegetables), protects mice from ALD development by activating intestinal *Ahr*. Data are represented as means ± SEM. *$P < 0.05$, Mann–Whitney test.

supplementation with AHR agonists provided a new therapeutic strategy for treating ALD.

Methods

Animals

$Ahr^{fl/fl}$ (stock no. 006203) and Villin-Cre (stock no. 021504) mice on a C57BL/6 background were purchased from Jackson Laboratory (Bar Harbor, ME) and bred in-house at China Pharmaceutical University. For IEC-specific *Ahr* disruption, $Ahr^{fl/fl}$ were crossed with Villin-Cre mice to obtain $Ahr^{\Delta IEC}$ mice. WT mice on a C57BL/6 background were obtained from Beijing Vital River Laboratory Animal Technology Company (Beijing, China). All mice were housed in the specific pathogen-free facility and maintained under a temperature-controlled (22°C–23°C) room with a 12:12-hour light/dark cycle. All animal procedures were performed in compliance with the guidelines of the Institutional Animal Care and Use Committee of China Pharmaceutical University (Nanjing, China).

Table 1. Demographic and Clinical Parameters of Controls and Patients With Alcoholic Liver Disease

Variables	Controls (n = 13)	Alcoholic liver disease (n = 13)
Sex, male, n (%), n = 26	12 (92.3)	12 (92.3)
Age, *y*, n = 26	49.07 (33–66)	52.8 (36–78)
ALT level, *U/L*, n = 23	19.6 (11.9–37.4)	30.5 (6.6–83.0)
AST level, *U/L*, n = 23	21.5 (13.0–28.0)	61.2 (19.6–237.0)
GGT level, *U/L*, n = 11		259.3 (18.3–932.1)
Albumin level, *g/dL*, n = 13		32.5 (24.5–41.5)
Bilirubin level, *mg/dL*, n = 13		40.4 (13.1–92.7)
Creatinine level, *mg/dL*, n = 13		65.9 (34.1–123.7)
INR, n = 11		1.3 (0.83–1.79)
Platelet count, 10^9/L, n = 13		115.6 (24.5–402.0)
MELD, n = 11		12.8 (7.0–18.0)
FIB-4, n = 11		7.2 (0.6–21.2)
FIB-4 > 3.25, n (%)		6 (46.2)
Prior length of alcohol abuse, n = 11		
10–20 y		2 (18.2%)
20–30 y		4 (36.4%)
>30 y		5 (45.4%)

ALT, alanine aminotransferase; AST, aspartate aminotransferase; FIB-4, fibrosis-4 index; GGT, γ-glutamyl transferase; INR, international normalized ratio; MELD, model for end-stage liver disease.

Animal Models

Age-matched female $Ahr^{fl/fl}$ and $Ahr^{\Delta IEC}$ littermates (age, 8–10 wk; weight, 20–22 g) were subjected to the chronic-plus-binge model.[23] In this model, 8-week-old mice (female) received a Lieber-DeCarli control liquid diet (F1259SP; Bio-Serv, Flemington, NJ) for 5 days and an ethanol liquid diet (F1258SP; Bio-Serv) for 10 days, and then were administered with a single binge of 5 g/kg ethanol (459844; Sigma-Aldrich, St. Louis, MO) on day 16. Pair-fed control mice ($Ahr^{fl/fl}$ and $Ahr^{\Delta IEC}$ littermates) received an isocaloric substitution of dextrose diet. For AHR agonist treatment, WT female mice were gavaged daily with a volume of 100 μL vehicle (dimethyl sulfoxide [DMSO] suspended in corn oil), 50 mg/kg I3C (105220; Aladdin, Shanghai, China), or 50 μg/kg FICZ (synthetized by Professor Yinan Zhang, Nanjing University of Chinese Medicine, Nanjing, China), starting on day 1 of the binge ethanol feeding model. I3C and FICZ were dissolved in a small volume of DMSO initially, and adjusted with corn oil to prepare the final concentrations before use.[12,29,47] When the mice were killed, plasma and appropriate tissues including liver, MLNs, intestine, and cecum were harvested. For IBA (I1754; Sigma-Aldrich) injection, WT female mice (age, 10 wk) were injected intraperitoneally with vehicle (phosphate-buffered saline [PBS]) or IBA (2.5% IBA diluted in PBS) at a dose of 2.5 mL/kg. Blood and liver tissues were collected at 24 or 48 hours after injection.

Human Samples

Alcoholic patients were enrolled in this study according to the pathologic examination results and inclusion criteria as described previously,[21,48] and written informed consent was signed by each patient and control. All of these participates did not take any antibiotics during the 2 weeks preceding the enrolment.

For *H. hepaticus* abundance in feces, patients with ALD (n = 13; 12 males/1 female; mean age, 52.8 y) were enrolled in this study. Thirteen healthy volunteers (social drinkers consuming <20 g/d; 12 males/1 female; mean age, 49.07 y) were recruited as controls. Baseline features of these subjects are shown in Table 1. Fecal samples were collected, frozen immediately, and stored at −80°C. The protocol was approved by the Ethics Committee of the Beijing Ditan Hospital, Capital Medical University (Beijing, China).

For intestinal AHR level analysis, duodenal tissues were collected with endoscopically normal duodenum from alcoholic patients (n = 6) and individuals without alcohol consumption (controls, n = 12). Patient characteristics are summarized in Table 2. This study protocol was approved by the Ethics Committee of the Sir Run Run Shaw Hospital, Nanjing Medical University (Nanjing, China).

Bacterial Cultures

H. hepaticus (ATCC51449) was a gift from Professor Quan Zhang's laboratory (Institute of Comparative Medicine, College of Veterinary Medicine, Yangzhou University, Yangzhou, Jiangsu, China).[49] The strain was cultured anaerobically on brucella agar (8241972; BD Difco, Detroit, MI) plates with 8% sheep blood (TX0030; Solarbio, Beijing, China) for 6 days. Bacteria collected and suspended in PBS (adjusted to optical density analysis at 600 nm [OD_{600}] = 1.0) were used for untargeted metabolomics.

Table 2. Demographic and Clinical Parameters of Controls and Alcoholic Patients

Variables	Controls (n = 12)	Alcoholic patients (n = 6)
Sex, male, n (%)	6 (50.0)	6 (100.0)
Age, *y*	36.7 (21–59)	51.2 (37–57)
ALT level, *U/L*	17.7 (8.0–25.0)	22.3 (15.0–29.0)
AST level, *U/L*	19.3 (14.0–29.0)	17 (15.0–20.0)
GGT level, *U/L*	26.1 (11.0–56.0)	30.7 (18.0–44.0)
Albumin level, *g/dL*	44.9 (41.2–48.8)	45.4 (43.3–51.2)
Bilirubin level, *μmol/L*	9.4 (5.8–13.2)	8.8 (5.3–14.3)
Creatinine level, *μmol/L*	69.3 (58.0–79.0)	62.2 (56.0–82.0)
INR	0.97 (0.89–1.10)	0.99 (0.89–1.04)
Platelet count, 10^9/L	225.7 (148.0–297.0)	215.7 (173.0–335.0)
FIB-4	0.71 (0.36–1.37)	1.19 (0.52–1.71)
Prior length of alcohol abuse, n = 6		
10–20 y		2 (16.7%)
20–30 y		1 (33.3%)
>30 y		3 (50.0%)

ALT, alanine aminotransferase; AST, aspartate aminotransferase; FIB-4, fibrosis-4 index; GGT, γ-glutamyl transferase; INR, international normalized ratio.

To determine the effect of metabolites for *H. hepaticus* growth in vitro, *H. hepaticus* was cultured on brucella agar plates containing 8% sheep blood with or without the metabolite. After 6 days of incubation, bacteria were collected and suspended in medium and growth was determined by OD_{600} measurement.

For *H. hepaticus* administration, WT female mice (age, 8 wk) subjected to the chronic-plus-binge model were orally gavaged every other day during the 15 days with either *H. hepaticus* (suspended in 200 μL broth, adjusted to OD_{600} = 1.0) or medium, respectively, as described.[49] At the end of the experiment, mice were killed and appropriate tissues were harvested.

Biochemical Assays

Blood was harvested from the inferior caval vein of mice to tubes containing anticoagulant (0.5 mol/L EDTA-Na_2), and centrifuged for 5 minutes (11,292 × g, 4°C) to obtain plasma. The levels of ALT, aspartate aminotransferase in plasma, and triglycerides in liver were determined using commercial kits (C009-2-1, C010-2-1, and A110-1-1, respectively; Nanjing Jiancheng Bioengineering Institute, Nanjing, Jiangsu, China).[50]

RNA Extraction and Real-Time qPCR

The total RNA from livers of mice was isolated using RNAiso Plus (9109; TaKaRa, Dalian, Liaoning, China) according to the methods described previously.[50] The complementary DNA was synthesized from 1 μg RNA by using a High Capacity complementary DNA reverse-transcription kit (R312-02; Vazyme, Nanjing, Jiangsu, China). qPCR was performed as described in our previous work[19,50] using SYBR Premix (Q331-02; Vazyme) according to the manufacturer's instructions on the ABI StepOnePlus real-time PCR machine (Applied Biosystems, Foster City, CA). All qPCR primers were synthesized by Sangon Biotech (Shanghai, China) and are shown in Table 3. The relative gene expression was calculated by the $2^{-\Delta\Delta Ct}$ method.

Bacterial DNA Isolation and qPCR for 16S, H. hepaticus, and H. ganmani

Bacterial genomic DNA was extracted from mice cecum content, livers, and MLNs as previously described.[19,50] The bacterial abundance was quantified by qPCR, and the value of the 16S rRNA gene was normalized to cecum weight, and the relative abundance of *H. hepaticus* and *H. ganmani* in cecum, livers, and MLNs were normalized to 16S.

16S rRNA Gene Sequencing and Analysis

Cecal DNA samples from each group were selected randomly for 16S rRNA gene sequencing and analysis.[19] The V4 region of the 16S rRNA gene was amplified and sequenced using the Illumina NovaSeq platform (Illumina, San Diego, CA) in Novogene Technology Co, Ltd (Beijing, China). Raw sequence data were analyzed with a pipeline[51] based on USEARCH[52] v10.0.240 (http://www.drive5.com/usearch) and VSEARCH[53] v2.13.6 (https://github.com/torognes/vsearch). Briefly, after a combination of sequences and removal of barcodes, UNOISE3[54] was performed to generate amplicon sequence variants. After sequence alignment by SILVA database[55] (Silva_123, http://www.drive5.com/usearch/manual/sintax_downloads.html), β-diversity was calculated with USEARCH. The principal coordinate analysis plot was generated based on Bray-Curtis distance. Then LEfSe[56] (http://huttenhower.sph.harvard.edu/galaxy) and the R package edgeR[57] were obtained for detecting differential taxons. All plots were drawn by R version 3.6.1 except those of LEfSe. The raw data reported here have been deposited in the National Center for Biotechnology Information Sequence Read Archive database (accession no. PRJNA663684).

Untargeted Metabolomics

Mice cecal contents were analyzed for untargeted metabolomics by using an ultrahigh performance liquid chromatography (UHPLC, 1290 Infinity LC; Agilent Technologies, Santa Clara, CA) coupled to a quadrupole time-of-flight (AB Sciex TripleTOF 6600; Applied Protein Technology, Shanghai, China). The analytes were separated on a 2.1 mm × 100 mm ACQUIY UPLC BEH 1.7-μm C18 column (Waters, Dublin, Ireland) and analyzed in both electrospray-positive and electrospray-negative ionization modes.

Table 3. Primers Used for Real-Time Reverse-Transcription PCR

Name	Sequence, 5'-3'
Primers for mouse	
Acaca-f	GGACAGACTGATCGCAGAGAAAG
Acaca-r	TGGAGAGCCCCACACACA
Acly-f	AGCAGACATAGTCAAAGTCCAG
Acly-r	AAGATTCAGTCCCAAGTCCAAG
Acox1-f	TCGCAGACCCTGAAGAAATC
Acox1-r	CCTGATTCAGCAAGGTAGGG
Adgre1-f	CATAAGCTGGGCAAGTGGTA
Adgre1-r	GGATGTACAGATGGGGGATG
Adh1-f	AGGCATTGTTGAGAGCGTTG
Adh1-r	CGAGGCATTAGCAGATCGC
Ahr-f	CTCCTTCTTGCAAATCCTGC
Ahr-r	GGCCAAGAGCTTCTTTGATG
Cd36-f	GCGACATGATTAATGGCACA
Cd36-r	CCTGCAAATGTCAGAGGAAA
Cpt1a-f	AGTGGCCTCACAGACTCCAG
Cpt1a-r	GCCCATGTTGTACAGCTTCC
Cxcl5-f	TGATCCCTGCAGGTCCACA
Cxcl5-r	CTGCGAGTGCATTCCGCTTA
Cxcl10-f	CCAAGTGCTGCCGTCATTTTC
Cxcl10-r	GGCTCGCAGGGATGATTTCAA
Cyp1a1-f	ACCCTTACAAGTATTTGGTCGT
Cyp1a1-r	GTCATCATGGTCATAACGTTGG
Cyp1a2-f	ATCCTGGAGATCTACCGATACA
Cyp1a2-r	TATGTAGATACAGCGCTCCTTG
Cyp1b1-f	CCAAGAATACGGTCGTTTTTGT
Cyp1b1-r	GTTAGCCTTGAAATTGCACTGA
Cyp2e1-f	CACCCTCCTCCTCGTATC
Cyp2e1-r	CGCTTTGCCAACTTGGTT
Dgat2-f	CGCAGCGAAAACAAGAATAA
Dgat2-r	GAAGATGTCTTGGAGGGCTG
Elovl1-f	CCATACATCCAGATGAGGTGAA
Elovl1-r	AGCACATGACAGCCATTCAG
Elovl5-f	CCTTGAAATAGGTACTAAGTGATGC
Elovl5-r	CTCCTTCTACATCCGCCTCT
Elovl7-f	GCAATCCTCCATGAAAAAGAACT
Elovl7-r	CCAGCCTACCAGAAGTATTTGTG
Fasn-f	CTCGCTTGTCGTCTGCCT
Fasn-r	ATGTCCACACCACCAATGAG
Il1b-f	TGTGAAATGCCACCTTTTGA
Il1b-r	GGTCAAAGGTTTGGAAGCAG
Il6-f	TAGTCCTTCCTACCCCAATTTCC
Il6-r	TTGGTCCTTAGCCACTCCTTC
Il17-f	CTGTCTCTCCCGCTACTG
Il17-r	CTAGCAGCTTCCTCTGGAA
Il22-f	AGGCATTGTTGAGAGCGTTG
Il22-r	CGAGGCATTAGCAGATCGC
Lgr5-f	GGACCAGATGCGATACCGC
Lgr5-r	CAGAGGCGATGTAGGAGACTG
Lipe-f	CCTGCAAGAGTATGTCACGC
Lipe-r	GGAGAGAGTCTGCAGGAACG
Lpl-f	CTGGTGGTCCTGGGAGTTT
Lpl-r	TCCTCAGCTGTGTCTTCAGG
Lrig1-f	TTGAGGACTTGACGAATCTGC
Lrig1-r	CTTGTTGTGCTGCAAAAAGAGAG
Ly6g-f	CATCCTTCTTGTGGTCCTACTGTGTG
Ly6g-r	TCTATCTCCAGAGCAACGCAAAATCC
Muc2-f	CCTTGCAGTCAAACTCAAAGT
Muc2-r	AAGTTTGCCCCTGGCTATGAC
Ocln-f	ATTTATGATGAACAGCCCCC
Ocln-r	CATAGTCAGATGGGGGTGGA
Srebf1-f	ACAGCGGTTTTGAACGACAT
Srebf1-r	GCTCTCAGGAGAGTTGGCAC
Tjp1-f	TGCAATTCCAAATCCAAACC
Tjp1-r	AGAGACAAGATGTCCGCCAG
Tjp2-f	TTTTTGAGCTTGTTGGCTTG
Tjp2-r	GTGATTTTCTTCAACCCGGA
Tnf-f	AGATGATCTGACTGCCTGGG
Tnf-r	CTGCTGCACTTTGGAGTGAT
18S-f	AGTCCCTGCCCTTTGTACACA
18S-r	CGATCCGAGGGCCTCACTA
Primers for bacteria	
Alistipes-f	ACATAGGGGGACTGAGAGGT
Alistipes-r	GCATGGCTGGTTCAGACTTG
A finegoldii-f	GTGAGGTAACGGCTCACCAA
A finegoldii-r	GCTCCTACACGTAGAAGCGT
A Indistinctus-f	GTGAGGTAACGGCTCACCAA
A Indistinctus-r	CGATACTTTCAAACAGGTACACGT
A timonensis-f	GTGAGGTAACGGCTCACCAA
A timonensis-r	CGTACTATACTTTCAGTCAGATACACG
Bacteroidetes-f	GGCGACCGGCGCACGGG
Bacteroidetes-r	GRCCTTCCTCTCAGAACCC
Bifidobacterium-f	TCGCGTCYGGTGTGAAAG
Bifidobacterium-r	CCACATCCAGCWTCCAC
Clostridium-f	ACGCTACTTGAGGAGGA
Clostridium-r	GAGCCGTAGCCTTTCACT
Enterococcus-f	AACCTACCCATCAGAGGG
Enterococcus-r	GACGTTCAGTTACTAACG
Firmicutes-f	GGAGYATGTGGTTTAATTCGA
Firmicutes-r	AGCTGACGACAACCATGCAC
H. hepaticus-f	TCGTGTCGTGAGATGTTGGG
H. hepaticus-r	TCCACCTCGCGATATTGCTC
H. ganmani-f	TGTGGAGCTTGTCTCTGCAG
H. ganmani-r	CCCAACATCTCACGACACGA
Prevotella-f	CACRGTAAACGATGGATGCC
Prevotella-r	GGTCGGGTTGCAGACC
16S-f	GTGSTGCAYGGYTGTCGTCA
16S-r	ACGTCRTCCMCACCTTCCTC

f, forward; r, reverse.

Metagenomics

DNA sample testing, library construction, and sequencing with an Illumina HiSeq platform were conducted at Novogene Technology Co, Ltd. The analyzing steps were described previously.[51] In short, quality control was performed with Kneaddata pipeline (https://bitbucket.org/biobakery/kneaddata) to exclude the host genome. Then, these clean reads were assembled to contigs via MEGAHIT,[58] and Prokka[59] was used for contigs identification in a conda environment of MetaWrap,[60] and CD-HIT[61] was used for nonredundant genes. A gene abundance table was generated through Salmon[62] and functional annotations of Kyoto Encyclopedia of Genes and Genomes (KEGG) Orthology by eggNOG-mapper[63] with its related database.

SCFA Quantification

Cecum content of SCFAs were analyzed based on previous method.[64] Briefly, samples (50 mg) were suspended in 200 μL distilled water and acidified with 50 μL (50%) sulfuric acid. Then, the solution was vortexed vigorously and extracted with diethyl ether. SCFAs were quantified by a gas chromatography Nexis GC-2030 (Shimadzu, Kyoto, Japan).

Staining Procedures

The liver samples were formalin-fixed and sectioned for H&E staining as described.[19] Frozen liver sections were stained with Oil red O.[19] Formalin-fixed intestinal samples were embedded in paraffin and stained with anti-AHR antibody (ab84833, 1:200; Abcam, Cambridge, MA) and anti-myeloperoxidase antibody (ab9535, 1:200; Abcam). All sections were scanned by Nano Zoomer 2.0 RS (Hamamatsu).[65]

Western Blot Analysis

Western blot analysis was performed as described in our previous work.[19] Briefly, intestine or liver tissues were lysed and the extracted protein was separated by sodium dodecyl sulfate–polyacrylamide gel electrophoresis, followed by transferring into a nitrocellulose membrane. The membranes were blocked and probed with antibodies against CYP2E1 (AB1252, 1:1000; Millipore, Bedford, MA) or actin (A5441, 1:5000; Sigma-Aldrich) overnight and then incubated with the corresponding secondary antibodies. The protein bands were quantified using Image J (National Institutes of Health, Bethesda, MD), normalized to actin.

Cell Culture Experiments

MODE-K cells (C495; Shanghai Hongshun Biotechnology Co, Ltd, Shanghai, China) were treated with vehicle (PBS) or ethanol (86, 100, and 200 mmol/L) for 24 hours for extraction of RNA and qPCR analysis. For *H. hepaticus* co-culture experiments, AML12 cells (CRL-2254; ATCC, Rockville, MD) were seeded in 12-well plates overnight, and subsequently exposed to *H. hepaticus* collected from the plates ($OD_{600} = 1$, suspended in cell culture medium, 100 μL/well). After incubation for 2 hours anaerobically, the plate was subjected to aerobic conditions for a total of 24 hours.[66] The treated cells were stained with Oil red O or extracted RNA for qPCR analysis.

Luciferase-Reporter Assay

AML12 cells were seeded in a 24-well plate and cultured for 12 hours before transfection with *Ahr* reporter plasmid (kindly provided by Professor Dalei Wu, Shandong University, China)[67] and pRL-TK Vector (E2241; Promega, Madison, WI). After 24 hours, cells were treated with AHR agonists (suspended in DMSO initially and diluted with medium). With another 24 hours of incubation, cells were washed with PBS and then lysed with lysis buffer (E1910; Promega). Luciferase activity was measured using a microplate reader (Tecan Spark, Männedorf, Switzerland) after adding luciferase reagent (E1910; Promega).

Isolation of IECs and Lamina Propria Cells

Small intestines were harvested immediately once mice were killed. After removal of all visible fat and Peyer's patches, all intestines were cut open longitudinally. Then, IECs and lamina propria cells were collected based on the protocol as described previously.[26]

Isolation of Kupffer Cells

Kupffer cells were isolated as described in our previous work.[68]

Organoid Culture

Intestinal organoids were derived from WT mice and cultured as described previously.[69–71] In brief, small intestine was harvested and flushed with cold Dulbecco's phosphate-buffered saline (DPBS). The intestine was cut longitudinally followed by removal of intestinal contents and villi. Intestine was washed and cut into 2- to 4-mm pieces, then tissues were collected after filtrating through a 70-μm cell strainer. After digestion in 2 mmol/L EDTA of DPBS for 30 minutes, intestine pieces were transferred into DPBS and shaken vigorously. After filtration through a 70-μm cell strainer 3 times, the crypts were harvested by centrifuging (600 $\times$ g, 5 min). Crypts were suspended in Matrigel (3432-010-01; R&D Biosystems, Minneapolis, MN) and cultured with IntestiCult OGM mouse basal medium (06000; Stemcell Technologies, Vancouver, Canada).

Microinjection of H. hepaticus Into Organoids

H. hepaticus was microinjected into the intestinal organoids as previously described.[71,72] Antibiotic-free mouse basal medium was refreshed every 3 days to remove antibiotics before injection. *H. hepaticus* was collected and suspended in antibiotic-free medium ($OD_{600} = 0.4$). Then, *H. hepaticus* with or without POPG (5 μg/mL) was microinjected into lumens of organoids with FastGreen dye (0.05%, wt/vol, F7252; Sigma-Aldrich), which is used to track the injected organoids. After 2 hours, fresh medium with nonpermeant gentamicin (5 μg/mL) was added to prevent the overgrowth of bacteria outside the organoids. After 4 days of incubation, the injected organoids were dissociated with 200 μL broth containing 0.5% saponin (SAE0073; Sigma-Aldrich) for 15 minutes with repeated pipetting on ice. The bacteria were released and cultured on plates with 8% sheep blood for 6 days to determine OD_{600} analysis.

Synthesis of FICZ

The starting materials were 1-Boc-3-(2-ethoxyl-2-oxoethyl)-indole and 1-Boc-2-chloro-3-formyl-indole, and FICZ was synthesized as described in the previous work.[73,74]

Statistical Analysis

Results in this study are expressed as means ± SEM. Statistical significance between 2 groups was determined by the Mann–Whitney test or an unpaired t test. All analyses were performed using GraphPad PRISM 7.0 (San Diego, CA). $P < 0.05$ was considered statistically significant. For untargeted metabolomics, significance between groups was identified based on the combination of variable influence on projection values (>1.0) and P values (<0.1).

All authors had access to the study data and reviewed and approved the final manuscript.

References

1. Avila MA, Dufour JF, Gerbes AL, Zoulim F, Bataller R, Burra P, Cortez-Pinto H, Gao B, Gilmore I, Mathurin P, Moreno C, Poznyak V, Schnabl B, Szabo G, Thiele M, Thursz MR. Recent advances in alcohol-related liver disease (ALD): summary of a Gut round table meeting. Gut 2020;69:764–780.
2. Szabo G, Kamath PS, Shah VH, Thursz M, Mathurin P, Meeting E-AJ. Alcohol-related liver disease: areas of consensus, unmet needs and opportunities for further study. Hepatology 2019;69:2271–2283.
3. Seitz HK, Bataller R, Cortez-Pinto H, Gao B, Gual A, Lackner C, Mathurin P, Mueller S, Szabo G, Tsukamoto H. Alcoholic liver disease. Nat Rev Dis Primers 2018;4:16.
4. Crabb DW, Im GY, Szabo G, Mellinger JL, Lucey MR. Diagnosis and treatment of alcohol-associated liver diseases: 2019 practice guidance from the American Association for the Study of Liver Diseases. Hepatology 2020;71:306–333.
5. Kiss EA, Vonarbourg C, Kopfmann S, Hobeika E, Finke D, Esser C, Diefenbach A. Natural aryl hydrocarbon receptor ligands control organogenesis of intestinal lymphoid follicles. Science 2011;334:1561–1565.
6. Rothhammer V, Quintana FJ. The aryl hydrocarbon receptor: an environmental sensor integrating immune responses in health and disease. Nat Rev Immunol 2019;19:184–197.
7. Fernandez-Salguero P, Pineau T, Hilbert DM, McPhail T, Lee SS, Kimura S, Nebert DW, Rudikoff S, Ward JM, Gonzalez FJ. Immune system impairment and hepatic fibrosis in mice lacking the dioxin-binding Ah receptor. Science 1995;268:722–726.
8. Li Y, Innocentin S, Withers DR, Roberts NA, Gallagher AR, Grigorieva EF, Wilhelm C, Veldhoen M. Exogenous stimuli maintain intraepithelial lymphocytes via aryl hydrocarbon receptor activation. Cell 2011;147:629–640.
9. Lee JS, Cella M, McDonald KG, Garlanda C, Kennedy GD, Nukaya M, Mantovani A, Kopan R, Bradfield CA, Newberry RD, Colonna M. AHR drives the development of gut ILC22 cells and postnatal lymphoid tissues via pathways dependent on and independent of Notch. Nat Immunol 2011;13:144–151.
10. Qiu J, Heller JJ, Guo X, Chen ZM, Fish K, Fu YX, Zhou L. The aryl hydrocarbon receptor regulates gut immunity through modulation of innate lymphoid cells. Immunity 2012;36:92–104.
11. Moura-Alves P, Fae K, Houthuys E, Dorhoi A, Kreuchwig A, Furkert J, Barison N, Diehl A, Munder A, Constant P, Skrahina T, Guhlich-Bornhof U, Klemm M, Koehler AB, Bandermann S, Goosmann C, Mollenkopf HJ, Hurwitz R, Brinkmann V, Fillatreau S, Daffe M, Tummler B, Kolbe M, Oschkinat H, Krause G, Kaufmann SH. AhR sensing of bacterial pigments regulates antibacterial defence. Nature 2014;512:387–392.
12. Metidji A, Omenetti S, Crotta S, Li Y, Nye E, Ross E, Li V, Maradana MR, Schiering C, Stockinger B. The environmental sensor AHR protects from inflammatory damage by maintaining intestinal stem cell homeostasis and barrier integrity. Immunity 2018;49:353–362 e5.
13. Bajaj JS. Alcohol, liver disease and the gut microbiota. Nat Rev Gastroenterol Hepatol 2019;16:235–246.
14. Sarin SK, Pande A, Schnabl B. Microbiome as a therapeutic target in alcohol-related liver disease. J Hepatol 2019;70:260–272.
15. Lang S, Schnabl B. Microbiota and fatty liver disease-the known, the unknown, and the future. Cell Host Microbe 2020;28:233–244.
16. Schnabl B, Brenner DA. Interactions between the intestinal microbiome and liver diseases. Gastroenterology 2014;146:1513–1524.
17. Chu H, Duan Y, Yang L, Schnabl B. Small metabolites, possible big changes: a microbiota-centered view of non-alcoholic fatty liver disease. Gut 2019;68:359–370.
18. Starkel P, Schnabl B. Bidirectional communication between liver and gut during alcoholic liver disease. Semin Liver Dis 2016;36:331–339.
19. Wang L, Fouts D, Starkel P, Hartmann P, Chen P, Llorente C, DePew J, Moncera K, Ho SB, Brenner DA, Hooper LV, Schnabl B. Intestinal REG3 lectins protect against alcoholic steatohepatitis by reducing mucosa-associated microbiota and preventing bacterial translocation. Cell Host Microbe 2016;19:227–239.
20. Llorente C, Jepsen P, Inamine T, Wang L, Bluemel S, Wang HJ, Loomba R, Bajaj JS, Schubert ML, Sikaroodi M, Gillevet PM, Xu J, Kisseleva T, Ho SB, DePew J, Du X, Sorensen HT, Vilstrup H, Nelson KE, Brenner DA, Fouts DE, Schnabl B. Gastric acid suppression promotes alcoholic liver disease by inducing overgrowth of intestinal *Enterococcus*. Nat Commun 2017;8:837.
21. Duan Y, Llorente C, Lang S, Brandl K, Chu H, Jiang L, White RC, Clarke TH, Nguyen K, Torralba M, Shao Y, Liu J, Hernandez-Morales A, Lessor L, Rahman IR, Miyamoto Y, Ly M, Gao B, Sun W, Kiesel R, Hutmacher F, Lee S, Ventura-Cots M, Bosques-Padilla F, Verna EC, Abraldes JG, Brown RS Jr, Vargas V, Altamirano J, Caballería J, Shawcross DL, Ho SB, Louvet A, Lucey MR, Mathurin P, Garcia-Tsao G, Bataller R, Tu XM, Eckmann L, van der Donk WA, Young R, Lawley TD, Stärkel P, Pride D, Fouts DE, Schnabl B. Bacteriophage targeting of gut bacterium attenuates alcoholic liver disease. Nature 2019;575:505–511.
22. Manfredo Vieira S, Hiltensperger M, Kumar V, Zegarra-Ruiz D, Dehner C, Khan N, Costa FRC, Tiniakou E, Greiling T, Ruff W, Barbieri A, Kriegel C, Mehta SS, Knight JR, Jain D, Goodman AL, Kriegel MA. Translocation of a gut pathobiont drives autoimmunity in mice and humans. Science 2018;359:1156–1161.
23. Bertola A, Mathews S, Ki SH, Wang H, Gao B. Mouse model of chronic and binge ethanol feeding (the NIAAA model). Nat Protoc 2013;8:627–637.
24. Hartmann P, Chen P, Wang HJ, Wang L, McCole DF, Brandl K, Stärkel P, Belzer C, Hellerbrand C, Tsukamoto H, Ho SB, Schnabl B. Deficiency of intestinal mucin-2 ameliorates experimental alcoholic liver disease in mice. Hepatology 2013;58:108–119.

25. Lieber CS. Relationships between nutrition, alcohol use, and liver disease. Alcohol Res Health 2003;27:220–231.
26. Hendrikx T, Duan Y, Wang Y, Oh JH, Alexander LM, Huang W, Starkel P, Ho SB, Gao B, Fiehn O, Emond P, Sokol H, van Pijkeren JP, Schnabl B. Bacteria engineered to produce IL-22 in intestine induce expression of REG3G to reduce ethanol-induced liver disease in mice. Gut 2019;68:1504–1515.
27. Alkhedaide AQ. Preventive effect of Juniperus procera extract on liver injury induced by lithocholic acid. Cell Mol Biol (Noisy-le-Grand) 2018;64:63–68.
28. Lian JS, Liu W, Hao SR, Guo YZ, Huang HJ, Chen DY, Xie Q, Pan XP, Xu W, Yuan WX, Li LJ, Huang JR. A serum metabonomic study on the difference between alcohol- and HBV-induced liver cirrhosis by ultraperformance liquid chromatography coupled to mass spectrometry plus quadrupole time-of-flight mass spectrometry. Chin Med J (Engl) 2011;124:1367–1373.
29. Wincent E, Bengtsson J, Mohammadi Bardbori A, Alsberg T, Luecke S, Rannug U, Rannug A. Inhibition of cytochrome P4501-dependent clearance of the endogenous agonist FICZ as a mechanism for activation of the aryl hydrocarbon receptor. Proc Natl Acad Sci U S A 2012;109:4479–4484.
30. Murray IA, Patterson AD, Perdew GH. Aryl hydrocarbon receptor ligands in cancer: friend and foe. Nat Rev Cancer 2014;14:801–814.
31. Stejskalova L, Dvorak Z, Pavek P. Endogenous and exogenous ligands of aryl hydrocarbon receptor: current state of art. Curr Drug Metab 2011;12:198–212.
32. Wrzosek L, Ciocan D, Hugot C, Spatz M, Dupeux M, Houron C, Lievin-Le Moal V, Puchois V, Ferrere G, Trainel N, Mercier-Nome F, Durand S, Kroemer G, Voican CS, Emond P, Straube M, Sokol H, Perlemuter G, Cassard A-M. Microbiota tryptophan metabolism induces aryl hydrocarbon receptor activation and improves alcohol-induced liver injury. Gut 2021;70:1299–1308.
33. Chow J, Mazmanian SK. A pathobiont of the microbiota balances host colonization and intestinal inflammation. Cell Host Microbe 2010;7:265–276.
34. Laharie D, Asencio C, Asselineau J, Bulois P, Bourreille A, Moreau J, Bonjean P, Lamarque D, Pariente A, Soulé JC, Charachon A, Coffin B, Perez P, Mégraud F, Zerbib F. Association between enterohepatic *Helicobacter* species and Crohn's disease: a prospective cross-sectional study. Aliment Pharmacol Ther 2009;30:283–293.
35. Bohr UR, Glasbrenner B, Primus A, Zagoura A, Wex T, Malfertheiner P. Identification of enterohepatic *Helicobacter* species in patients suffering from inflammatory bowel disease. J Clin Microbiol 2004;42:2766–2768.
36. Nilsson I, Kornilovs'ka I, Lindgren S, Å Ljungh, Wadström T. Increased prevalence of seropositivity for non-gastric *Helicobacter* species in patients with autoimmune liver disease. J Med Microbiol 2003;52:949–953.
37. Yang J, Ji S, Zhang Y, Wang J. *Helicobacter hepaticus* infection in primary hepatocellular carcinoma tissue. Singapore Med J 2013;54:451–457.
38. Shimoyama T, Takahashi R, Abe D, Mizuki I, Endo T, Fukuda S. Serological analysis of *Helicobacter hepaticus* infection in patients with biliary and pancreatic diseases. J Gastroenterol Hepatol 2010;25(Suppl 1):S86–S89.
39. Hamada T, Yokota K, Ayada K, Hirai K, Kamada T, Haruma K, Chayama K, Oguma K. Detection of *Helicobacter hepaticus* in human bile samples of patients with biliary disease. Helicobacter 2009;14:545–551.
40. Fan Y, Pedersen O. Gut microbiota in human metabolic health and disease. Nat Rev Microbiol 2021;19:55–71.
41. Aron-Wisnewsky J, Vigliotti C, Witjes J, Le P, Holleboom AG, Verheij J, Nieuwdorp M, Clément K. Gut microbiota and human NAFLD: disentangling microbial signatures from metabolic disorders. Nat Rev Gastroenterol Hepatol 2020;17:279–297.
42. Da Silva HE, Teterina A, Comelli EM, Taibi A, Arendt BM, Fischer SE, Lou W, Allard JP. Nonalcoholic fatty liver disease is associated with dysbiosis independent of body mass index and insulin resistance. Sci Rep 2018;8:1466.
43. Addolorato G, Mirijello A, Leggio L, Ferrulli A, Landolfi R. Management of alcohol dependence in patients with liver disease. CNS Drugs 2013;27:287–299.
44. Leggio L, Lee MR. Treatment of alcohol use disorder in patients with alcoholic liver disease. Am J Med 2017;130:124–134.
45. Shin D, Shin JY, McManus MT, Ptácek LJ, Fu YH. Dicer ablation in oligodendrocytes provokes neuronal impairment in mice. Ann Neurol 2009;66:843–857.
46. Kihara A. Very long-chain fatty acids: elongation, physiology and related disorders. J Biochem 2012;152:387–395.
47. Singh NP, Singh UP, Rouse M, Zhang J, Chatterjee S, Nagarkatti PS, Nagarkatti M. Dietary indoles suppress delayed-type hypersensitivity by Inducing a switch from proinflammatory Th17 cells to anti-inflammatory regulatory T cells through regulation of microRNA. J Immunol 2016;196:1108–1122.
48. Brandl K, Hartmann P, Jih LJ, Pizzo DP, Argemi J, Ventura-Cots M, Coulter S, Liddle C, Ling L, Rossi SJ, DePaoli AM, Loomba R, Mehal WZ, Fouts DE, Lucey MR, Bosques-Padilla F, Mathurin P, Louvet A, Garcia-Tsao G, Verna EC, Abraldes JG, Brown RS Jr, Vargas V, Altamirano J, Caballería J, Shawcross D, Stärkel P, Ho SB, Bataller R, Schnabl B. Dysregulation of serum bile acids and FGF19 in alcoholic hepatitis. J Hepatol 2018;69:396–405.
49. Cao S, Zhu C, Feng J, Zhu L, Yin J, Xu Y, Yang H, Huang Y, Zhang Q. *Helicobacter hepaticus* infection induces chronic hepatitis and fibrosis in male BALB/c mice via the activation of NF-κB, Stat3, and MAPK signaling pathways. Helicobacter 2020;25:e12677.
50. Qian M, Hu H, Yao Y, Zhao D, Wang S, Pan C, Duan X, Gao Y, Liu J, Zhang Y, Yang S, Qi LW, Wang L. Coordinated changes of gut microbiome and lipidome differentiates nonalcoholic steatohepatitis (NASH) from isolated steatosis. Liver Int 2020;40:622–637.

51. Liu YX, Qin Y, Chen T, Lu M, Qian X, Guo X, Bai Y. A practical guide to amplicon and metagenomic analysis of microbiome data. Protein Cell 2021;12:315–330.
52. Edgar RC. Search and clustering orders of magnitude faster than BLAST. Bioinformatics 2010;26:2460–2461.
53. Rognes T, Flouri T, Nichols B, Quince C, Mahe F. VSEARCH: a versatile open source tool for metagenomics. PeerJ 2016;4:e2584.
54. Edgar RC. UNOISE2: improved error-correction for Illumina 16S and ITS amplicon sequencing. bioRxiv 2016. https://doi.org/10.1101/081257.
55. Yilmaz P, Parfrey LW, Yarza P, Gerken J, Pruesse E, Quast C, Schweer T, Peplies J, Ludwig W, Glöckner FO. The SILVA and "All-species Living Tree Project (LTP)" taxonomic frameworks. Nucleic Acids Res 2013;42:D643–D648.
56. Segata N, Izard J, Waldron L, Gevers D, Miropolsky L, Garrett WS, Huttenhower C. Metagenomic biomarker discovery and explanation. Genome Biol 2011;12:R60.
57. Robinson MD, McCarthy DJ, Smyth GK. edgeR: a Bioconductor package for differential expression analysis of digital gene expression data. Bioinformatics 2010;26:139–140.
58. Li D, Liu CM, Luo R, Sadakane K, Lam TW. MEGAHIT: an ultra-fast single-node solution for large and complex metagenomics assembly via succinct de Bruijn graph. Bioinformatics 2015;31:1674–1676.
59. Seemann T. Prokka: rapid prokaryotic genome annotation. Bioinformatics 2014;30:2068–2069.
60. Uritskiy GV, DiRuggiero J, Taylor J. MetaWRAP-a flexible pipeline for genome-resolved metagenomic data analysis. Microbiome 2018;6:158.
61. Fu L, Niu B, Zhu Z, Wu S, Li W, CD-HIT. accelerated for clustering the next-generation sequencing data. Bioinformatics 2012;28:3150–3152.
62. Patro R, Duggal G, Love MI, Irizarry RA, Kingsford C. Salmon provides fast and bias-aware quantification of transcript expression. Nat Methods 2017;14:417–419.
63. Huerta-Cepas J, Forslund K, Coelho LP, Szklarczyk D, Jensen LJ, von Mering C, Bork P. Fast genome-wide functional annotation through orthology assignment by eggNOG-Mapper. Mol Biol Evol 2017;34:2115–2122.
64. Zhang S, Wang H, Zhu MJ. A sensitive GC/MS detection method for analyzing microbial metabolites short chain fatty acids in fecal and serum samples. Talanta 2019;196:249–254.
65. Wang L, Mazagova M, Pan C, Yang S, Brandl K, Liu J, Reilly SM, Wang Y, Miao Z, Loomba R, Lu N, Guo Q, Liu J, Yu RT, Downes M, Evans RM, Brenner DA, Saltiel AR, Beutler B. YIPF6 controls sorting of FGF21 into COPII vesicles and promotes obesity. Proc Natl Acad Sci U S A 2019;116:15184–15193.
66. Long X, Wong CC, Tong L, Chu ESH, Ho Szeto C, Go MYY, Coker OO, Chan AWH, Chan FKL, Sung JJY, Yu J. *Peptostreptococcus anaerobius* promotes colorectal carcinogenesis and modulates tumour immunity. Nat Microbiol 2019;4:2319–2330.
67. Wu D, Potluri N, Kim Y, Rastinejad F. Structure and dimerization properties of the aryl hydrocarbon receptor PAS-A domain. Mol Cell Biol 2013;33:4346–4356.
68. Mazagova M, Wang L, Anfora AT, Wissmueller M, Lesley SA, Miyamoto Y, Eckmann L, Dhungana S, Pathmasiri W, Sumner S, Westwater C, Brenner DA, Schnabl B. Commensal microbiota is hepatoprotective and prevents liver fibrosis in mice. FASEB J 2015;29:1043–1055.
69. Qu M, Xiong L, Lyu Y, Zhang X, Shen J, Guan J, Chai P, Lin Z, Nie B, Li C. Establishment of intestinal organoid cultures modeling injury-associated epithelial regeneration. Cell Res 2021;31:259–271.
70. Sato T, Vries RG, Snippert HJ, van de Wetering M, Barker N, Stange DE, van Es JH, Abo A, Kujala P, Peters PJ, Clevers H. Single Lgr5 stem cells build crypt-villus structures in vitro without a mesenchymal niche. Nature 2009;459:262–265.
71. Pleguezuelos-Manzano C, Puschhof J, Rosendahl Huber A, van Hoeck A. Mutational signature in colorectal cancer caused by genotoxic pks(+) *E. coli*. Nature 2020;580:269–273.
72. Bartfeld S, Bayram T, van de Wetering M, Huch M, Begthel H, Kujala P, Vries R, Peters PJ, Clevers H. *In vitro* expansion of human gastric epithelial stem cells and their responses to bacterial infection. Gastroenterology 2015;148:126–136.e6.
73. Sekine D, Okeda S, Hosokawa S. Concise synthesis of 6-formylindolo[3,2-b]carbazole (FICZ). Chem Lett 2014;43:1932–1934.
74. Bergman JTaJ. Synthesis of 6-formylindolo[3,2-b]carbazole, an extremely potent ligand for the aryl hydrogen (Ah) receptor. Tetrahedron Lett 1998;39:1619–1622.

Received November 19, 2020. Accepted August 18, 2021.

Correspondence
Address correspondence to: Lirui Wang, PhD, Institute of Modern Biology, Nanjing University, 22 Hankou Road, Gulou District, Nanjing, 210093 China. e-mail: wanglirui@nju.edu.cn.

CRediT Authorship Contributions

Minyi Qian (Data curation: Lead; Formal analysis: Lead; Funding acquisition: Supporting; Investigation: Supporting; Methodology: Equal; Writing – original draft: Lead)

Jun Liu (Data curation: Equal; Formal analysis: Equal; Investigation: Supporting; Methodology: Equal)

Danyang Zhao (Data curation: Equal; Formal analysis: Equal; Investigation: Supporting; Methodology: Equal)

Pengpeng Cai (Resources: Supporting)

Chuyue Pan (Data curation: Supporting)

wenxin Jia (Writing – original draft: Supporting)

Yingsheng Gao (Data curation: Supporting)

Yufei Zhang (Data curation: Supporting)

Nan Zhang (Resources: Supporting)

Yinan Zhang (Resources: Supporting)

Quan Zhang (Resources: Supporting)

Dalei Wu (Resources: Supporting)

Chengjie Shan (Methodology: Supporting)

Meilin Zhang (Methodology: Supporting)

Bernd Schnabl (Funding acquisition: Supporting; Supervision: Supporting; Writing – review & editing: Supporting)

Song Yang (Resources: Supporting)
Xu Shen (Resources: Supporting; Supervision: Equal)
Lirui Wang (Conceptualization: Lead; Formal analysis: Lead; Funding acquisition: Lead; Investigation: Lead; Methodology: Lead; Project administration: Lead; Supervision: Lead; Writing – original draft: Supporting; Writing – review & editing: Lead)

Conflicts of interest

These authors disclose the following: Bernd Schnabl has consulted for Ferring Research Institute, Intercept Pharmaceuticals, HOST Therabiomics, Mabwell Therapeutics, and Patara Pharmaceuticals, and his institution (University of California San Diego) has received grant support from BiomX, NGM Biopharmaceuticals, CymaBay Therapeutics, Synlogic Operating Company, and Axial Biotherapeutics. The remaining authors disclose no conflicts.

Funding

Supported by the National Natural Science Foundation of China grant 82070602 (L.W.), "Double First-Class" University Project grants CPU2018GF10 and CPU2018GY31 (L.W.), National Key Research and Development Program of China grants 2018YFC1704900 and 2018YFC1704905 (L.W.), Natural Science Foundation of Jiangsu Province grant SBK2020040688 (M.Q.), National Natural Science Foundation of China grant 31700114 (D.W.), and National Science and Technology Major Project grant 2018ZX10715-005 (S.Y.). Also supported in part by National Institutes of Health grant P30 DK120515 (B.S.).